Transverse momentum dependence of D-meson production in Pb-Pb collisions at √sNN=2.76 TeV

(ALICE Collaboration) Adam, J.; ...; Antičić, Tome; ...; Erhardt, Filip; ...; Gotovac, Sven; ...; Mudnić, Eugen; ...; ...

Source / Izvornik: **Journal of High Energy Physics, 2016, 2016**

Journal article, Published version
Rad u časopisu, Objavljena verzija rada (izdavačev PDF)

https://doi.org/10.1007/JHEP03(2016)081

Permanent link / Trajna poveznica: https://urn.nsk.hr/urn:nbn:hr:217:611808

Published for SISSA by Springer

Received: October 5, 2015
Revised: December 18, 2015
Accepted: February 3, 2016
Published: March 14, 2016

Transverse momentum dependence of D-meson production in Pb-Pb collisions at $\sqrt{s_{NN}} = 2.76$ TeV

The ALICE collaboration

E-mail: ALICE-publications@cern.ch

Abstract: The production of prompt charmed mesons D^0, D^+ and D^{*+}, and their antiparticles, was measured with the ALICE detector in Pb-Pb collisions at the centre-of-mass energy per nucleon pair, $\sqrt{s_{NN}}$, of 2.76 TeV. The production yields for rapidity $|y| < 0.5$ are presented as a function of transverse momentum, p_T, in the interval 1–36 GeV/c for the centrality class 0–10% and in the interval 1–16 GeV/c for the centrality class 30–50%. The nuclear modification factor R_{AA} was computed using a proton-proton reference at $\sqrt{s} = 2.76$ TeV, based on measurements at $\sqrt{s} = 7$ TeV and on theoretical calculations. A maximum suppression by a factor of 5–6 with respect to binary-scaled pp yields is observed for the most central collisions at p_T of about 10 GeV/c. A suppression by a factor of about 2–3 persists at the highest p_T covered by the measurements. At low p_T (1–3 GeV/c), the R_{AA} has large uncertainties that span the range 0.35 (factor of about 3 suppression) to 1 (no suppression). In all p_T intervals, the R_{AA} is larger in the 30–50% centrality class compared to central collisions. The D-meson R_{AA} is also compared with that of charged pions and, at large p_T, charged hadrons, and with model calculations.

Keywords: Heavy ion Experiments, Quark gluon plasma, Charm physics

ArXiv ePrint: 1509.06888

doi:10.1007/JHEP03(2016)081

JHEP03(2016)081

Contents

JHEP03(2016)081

1 Introduction

A state of strongly-interacting matter characterised by high energy density and temperature is predicted to be formed in ultra-relativistic collisions of heavy nuclei. According to calculations using Quantum Chromodynamics (QCD) on the lattice, these extreme conditions lead to the formation of a Quark-Gluon Plasma (QGP) state, in which quarks and gluons are deconfined, and chiral symmetry is partially restored (see e.g. [1–4]).

Heavy quarks are produced in the hard scattering processes that occur in the early stage of the collision between partons of the incoming nuclei. Their production is characterised by a timescale $\Delta t < 1/(2\,m_{\mathrm{c,b}})$, $\sim 0.1\,\mathrm{fm}/c$ for charm and $\sim 0.01\,\mathrm{fm}/c$ for beauty quarks, that is shorter than the formation time of the QGP medium, about $0.3\,\mathrm{fm}/c$ at Large Hadron Collider (LHC) energies [5]. They can successively interact with the constituents of the medium and lose part of their energy, via inelastic processes (gluon radiation) [6, 7] or elastic scatterings (collisional processes) [8–10]. Energy loss can be studied using the

nuclear modification factor $R_{\rm AA}$, which compares the transverse-momentum ($p_{\rm T}$) differential production yields in nucleus-nucleus collisions ($\mathrm{d}N_{\rm AA}/\mathrm{d}p_{\rm T}$) with the cross section in proton-proton collisions ($\mathrm{d}\sigma_{\rm pp}/\mathrm{d}p_{\rm T}$) scaled by the average nuclear overlap function ($\langle T_{\rm AA}\rangle$)

$$R_{\rm AA}(p_{\rm T}) = \frac{1}{\langle T_{\rm AA}\rangle} \cdot \frac{\mathrm{d}N_{\rm AA}/\mathrm{d}p_{\rm T}}{\mathrm{d}\sigma_{\rm pp}/\mathrm{d}p_{\rm T}} \,. \tag{1.1}$$

The average nuclear overlap function $\langle T_{\rm AA}\rangle$ over a centrality class is proportional to the number of binary nucleon-nucleon collisions per A-A collision in that class and it can be estimated via Glauber model calculations [11, 12].

According to QCD calculations, quarks are expected to lose less energy than gluons because their coupling to the medium is smaller [6, 7]. In the energy regime of the LHC, light-flavour hadrons with $p_{\rm T}$ ranging from 5 to 20 GeV/c originate predominantly from gluons produced in hard scattering processes, while for larger $p_{\rm T}$ they originate mainly from light quarks (see e.g. [13]). Charmed mesons, instead, provide an experimental tag for a quark parent at all momenta. Therefore, the comparison of the heavy-flavour hadron $R_{\rm AA}$ with that of pions is expected to be sensitive to the colour-charge dependence of energy loss. However, other aspects than the energy loss, like the parton $p_{\rm T}$ spectrum and fragmentation into hadrons, influence the nuclear modification factor (see e.g. [13, 14]). The effect of the colour-charge dependence of the energy loss should be then studied via the comparison with model calculations, that include the description of the aforementioned aspects.

In addition, several mass-dependent effects are predicted to influence the energy loss for quarks (see [15] for a recent review). The dead-cone effect should reduce small-angle gluon radiation for quarks that have moderate energy-over-mass values, i.e. for c and b quarks with momenta up to about 10 and 30 GeV/c, respectively [16–22]. Likewise, collisional energy loss is predicted to be reduced for heavier quarks, because the spatial diffusion coefficient, which regulates the momentum transfers with the medium, scales with the inverse of the quark mass for a given quark momentum [23]. In particular, the study of D mesons from low-$p_{\rm T}$ to high-$p_{\rm T}$ allows to study the variation of the energy loss for different charm quark velocity: from a non-relativistic regime to an highly relativistic one. Low-momentum heavy quarks, including those shifted to low momentum by parton energy loss, could participate in the collective expansion of the system as a consequence of multiple interactions [24, 25]. It was also suggested that low-momentum heavy quarks could hadronise not only via fragmentation in the vacuum, but also via the mechanism of recombination with other quarks from the medium [25, 26].

The nuclear modification factor of heavy-flavour production was first studied at the Relativistic Heavy Ion Collider (RHIC). The PHENIX and STAR Collaborations reported measurements using heavy-flavour decay electrons and muons in Au-Au and Cu-Cu collisions at centre-of-mass energy per nucleon pair, $\sqrt{s_{\rm NN}} = 200$ GeV [27–30]. A suppression with respect to binary scaling was observed for $p_{\rm T}$ larger than about 3 GeV/c, reaching a minimum $R_{\rm AA}$ of about 0.2–0.3 in the interval $4 < p_{\rm T} < 6$ GeV/c. The STAR Collaboration recently measured the $R_{\rm AA}$ of D^0 mesons in Au-Au collisions for the interval $0 < p_{\rm T} < 6$ GeV/c [31]. At $p_{\rm T}$ of about 5–6 GeV/c the $R_{\rm AA}$ value is similar to that observed

JHEP03(2016)081

for electrons from heavy-flavour decays and the $R_{\rm AA}$ increases towards low $p_{\rm T}$, reaching a maximum value of about 1.5 at 1–2 GeV/c. This feature is described by heavy-flavour transport calculations that include radial flow and a contribution due to recombination in the charm hadronisation process [31].

A first measurement of the production of prompt D mesons at mid-rapidity in the $p_{\rm T}$ interval 2–16 GeV/c was published, using the Pb-Pb data at $\sqrt{s_{\rm NN}} = 2.76$ TeV collected in 2010 during LHC Run 1 [32]. A minimum $R_{\rm AA}$ of about 0.2–0.3 was measured at $p_{\rm T}$ of about 10 GeV/c for the 20% most central collisions. The measurement of D-meson production in p-Pb collisions at $\sqrt{s_{\rm NN}} = 5.02$ TeV, showing an $R_{\rm pPb}$ compatible with unity, has provided clear evidence that the suppression with respect to binary-scaled pp cross sections, observed in Pb-Pb collisions, cannot be attributed to cold nuclear matter effects for $p_{\rm T}$ larger than 2 GeV/c and is, thus, caused by final-state interactions in the hot and dense medium [33].

In Pb-Pb collisions, the nuclear modification factor at low $p_{\rm T}$ results from the interplay of different effects occurring in the initial and in the final state. The measured D-meson nuclear modification factor in p-Pb collisions, although consistent with unity, is also described within uncertainties by calculations that include substantial initial-state effects, such as parton shadowing or saturation [33], that could manifest as a reduction of the yields in Pb-Pb (and thus of the $R_{\rm AA}$) by up to 50% at low $p_{\rm T}$. In addition, the measurement of a significant azimuthal anisotropy of D-meson production, with respect to the estimated direction of the reaction plane in non-central Pb-Pb collisions, indicates that charm quarks participate in the collective expansion of the medium [34, 35]. Therefore, radial flow could play a relevant role as well. In order to investigate these aspects, it is important to have a precise measurement of $R_{\rm AA}$ down to low $p_{\rm T}$. In the high-$p_{\rm T}$ region, where parton energy loss is expected to be dominated by radiative processes, the extension of the D-meson $R_{\rm AA}$ beyond 20 GeV/c would provide the first measurement of identified-hadron $R_{\rm AA}$ at such high $p_{\rm T}$.

In this article we present the measurement of $p_{\rm T}$-differential yields and nuclear modification factors of prompt $\rm D^0$, $\rm D^+$ and $\rm D^{*+}$ mesons (including their antiparticles), reconstructed via their hadronic decays in Pb-Pb collisions at $\sqrt{s_{\rm NN}} = 2.76$ TeV, using the data sample recorded in 2011. For central collisions, the integrated luminosity is larger by a factor of about 10 than that used for the previously published results [32]. This allows us to extend the measurement of $R_{\rm AA}$ to lower and higher $p_{\rm T}$ (from 2–16 GeV/c to 1–36 GeV/c), to improve its precision, and to perform the study in a narrower class of the most central collisions (10% most central instead of 20% most central).

The article is organised as follows: the experimental apparatus is described in section 2, together with the data sample. In section 3, the D-meson decay reconstruction and all corrections applied to the yields are presented, along with the procedure used to obtain the pp reference at $\sqrt{s} = 2.76$ TeV. In section 4 the systematic uncertainties are discussed. The results for the 0–10% (central) and 30–50% (semi-peripheral) centrality classes are presented in section 5. In the same section results obtained in Pb-Pb collisions are compared with the nuclear modification factor measured in p-Pb collisions at $\sqrt{s_{\rm NN}} = 5.02$ TeV. A comparison with charged pions, charged particles (ch) and with theoretical model predic-

JHEP03(2016)081

Centrality class	$\langle T_{\rm AA} \rangle$ (mb^{-1})	$N_{\rm events}$	$L_{\rm int}$ (μb^{-1})
0–10%	23.44 ± 0.76	16.4×10^6	21.3 ± 0.7
30–50%	3.87 ± 0.18	9.0×10^6	5.8 ± 0.2

Table 1. Average of the nuclear overlap function, number of events and integrated luminosity for the two centrality classes used in the analysis. The uncertainty on the integrated luminosity stems from the uncertainty of the hadronic Pb-Pb cross section from the Glauber model [39].

tions is also reported. These comparisons are presented in terms of the ratio $R_{\rm AA}^{\rm D}/R_{\rm AA}^{\pi,\,ch}$ as well. Conclusions are drawn in section 6.

2 Experimental apparatus and data sample

The ALICE experimental apparatus [36] is composed of various detectors for particle reconstruction and identification at mid-rapidity ($|\eta| < 0.9$), a forward muon spectrometer ($-4 < \eta < -2.5$) and a set of forward-backward detectors for triggering and event characterization. The detector performance for measurements in pp, p-Pb and Pb-Pb collisions from the LHC Run 1 is presented in [37].

The main detector components used in this analysis are the V0 detector, the Inner Tracking System (ITS), the Time Projection Chamber (TPC) and the Time Of Flight (TOF) detector, which are located inside a large solenoidal magnet providing a uniform magnetic field of 0.5 T parallel to the LHC beam direction (z axis in the ALICE reference system) and the Zero Degree Calorimeter (ZDC), located at $\pm$114 m from the interaction point.

Pb-Pb collision data were recorded with a minimum-bias interaction trigger based on information from the V0 detector, which consists of two scintillator arrays covering the full azimuth in the pseudorapidity intervals $-3.7 < \eta < -1.7$ and $2.8 < \eta < 5.1$ [38]. The trigger logic required the coincidence of signals on both sides of the detector. An online selection based on the V0 signal amplitudes was used to enhance the sample of central and mid-central collisions through two separate trigger classes. The scintillator arrays have an intrinsic time resolution better than 0.5 ns, and their timing information was used together with that from the ZDCs for offline rejection of events produced by the interaction of the beams with residual gas in the vacuum pipe. Only events with a reconstructed interaction point (primary vertex) within $\pm$10 cm from the centre of the detector along the beam line were used in the analysis.

Collisions were divided into centrality classes, determined from the sum of the V0 signal amplitudes and defined in terms of percentiles of the total hadronic Pb-Pb cross section. In order to relate the centrality classes to the collision geometry, the distribution of the V0 summed amplitudes was fitted with a function based on the Glauber model [11, 12] combined with a two-component model for particle production [39]. The centrality classes used in the analysis are reported in table 1, together with the average of the nuclear overlap function $T_{\rm AA}$, the number of events in each class ($N_{\rm events}$) and the integrated luminosity.

JHEP03(2016)081

The charged-particle tracks used to reconstruct the decay of D mesons were measured in the TPC and ITS. The tracking algorithm, based on a Kalman filter [40], starts from three-dimensional space points in the TPC, a large cylindrical drift detector with both total length and diameter of about 5 m, covering the pseudorapidity range $|\eta| < 0.9$ with full azimuthal acceptance [41]. Tracks are reconstructed in the TPC with up to 159 space points and with a measurement of the specific ionisation energy loss $\mathrm{d}E/\mathrm{d}x$ with a resolution of about 6%.

Hits in the ITS are associated to the prolongation of the TPC tracks, forming the global tracks. The ITS consists of six cylindrical layers of silicon detectors [42]. The two innermost layers, placed at 3.9 and 7.6 cm from the beam line, consist of Silicon Pixel Detectors (SPD). The third and fourth layers use Silicon Drift Detectors (SDD) and the two outermost layers contain double-sided Silicon Strip Detectors (SSD). The effective spatial resolutions, including the intrinsic detector resolutions and residual mis-alignments, are about 14, 40 and 25 μm, for SPD, SDD and SSD, respectively, along the most precise direction ($r\varphi$) [42].

Global tracks are used to reconstruct the primary interaction vertex and the secondary vertices of D-meson decays. The transverse momentum resolution for global tracks ranges from about 1% at $p_{\mathrm{T}} = 1\,\mathrm{GeV}/c$ to about 2% at $10\,\mathrm{GeV}/c$, both in pp and Pb-Pb collisions. The spatial precision of global tracks is quantified by the resolution on the impact parameter d_0, which is the signed distance of closest approach between the track and the primary vertex in the xy-plane transverse to the beam direction. In Pb-Pb collisions, the d_0 resolution is better than 65 μm for tracks with a transverse momentum larger than $1\,\mathrm{GeV}/c$ and reaches 20 μm for $p_{\mathrm{T}} > 20\,\mathrm{GeV}/c$ [37].

The TOF detector is an array of Multi-Gap Resistive Plate Chambers positioned at a distance of about 370 cm from the beam line and covering the full azimuth over the pseudorapidity interval $|\eta| < 0.9$. TOF particle identification is based on the difference between the particle arrival time at the TOF detector and a start time determined using the arrival time of all particles of the event with a χ^2 minimization [43]. The resolution (σ) of the time-of-flight measurement is about 80 ps for pions at $p_{\mathrm{T}} = 1\,\mathrm{GeV}/c$ in the Pb-Pb collision centrality intervals used in this analysis. TOF provides charged-particle identification in the intermediate momentum range, with a 3σ separation up to about $2.5\,\mathrm{GeV}/c$ for pions and kaons, and up to about $4\,\mathrm{GeV}/c$ for kaons and protons [37].

3 Data analysis

3.1 D-meson reconstruction

D^0, D^+ and D^{*+} mesons, and their antiparticles, were reconstructed via their hadronic decay channels $\mathrm{D}^0 \to \mathrm{K}^-\pi^+$ (weak decay with branching ratio, BR, of $3.88 \pm 0.05\%$), $\mathrm{D}^+ \to \mathrm{K}^-\pi^+\pi^+$ (weak decay, BR of $9.13 \pm 0.19\%$) and $\mathrm{D}^{*+} \to \mathrm{D}^0\pi^+$ (strong decay, BR of $67.7 \pm 0.05\%$) followed by $\mathrm{D}^0 \to \mathrm{K}^-\pi^+$ [44]. D^0 and D^+ mesons have mean proper decay lengths ($c\tau$) of 123 and 312 μm, respectively [44]. In the case of the D^{*+}, the decay topology of the produced D^0 was exploited. The transverse momentum of the soft pions produced in the D^{*+} decays typically ranges from 0.1 to $1.5\,\mathrm{GeV}/c$, depending on the D^{*+} p_{T}.

JHEP03(2016)081

D^0 and D^+ candidates were formed using pairs and triplets of tracks with the correct charge-sign combination, requiring $|\eta| < 0.8$, $p_{\mathrm{T}} > 0.4\,\mathrm{GeV}/c$, at least 70 associated space points (out of a maximum of 159) and fit quality $\chi^2/\mathrm{ndf} < 2$ in the TPC, and at least two hits (out of six) in the ITS, out of which at least one in either of the two SPD layers. D^{*+} candidates were formed by combining D^0 candidates with tracks with $p_{\mathrm{T}} > 0.1\,\mathrm{GeV}/c$ and at least three hits in the ITS, out of which at least one in the SPD.

The aforementioned track selection limits the D-meson acceptance in rapidity. The acceptance drops steeply to zero for $|y| > 0.5$ at low p_{T} and $|y| > 0.8$ for $p_{\mathrm{T}} > 5\,\mathrm{GeV}/c$. A p_{T}-dependent fiducial acceptance cut, $|y_{\mathrm{D}}|<y_{\mathrm{fid}}(p_{\mathrm{T}})$, was therefore applied to the D-meson rapidity. The cut value, $y_{\mathrm{fid}}(p_{\mathrm{T}})$, increases from 0.5 to 0.8 in the range $0<p_{\mathrm{T}}<5\,\mathrm{GeV}/c$ according to a second-order polynomial function and with a constant value of 0.8 for $p_{\mathrm{T}} > 5\,\mathrm{GeV}/c$.

The selection of the decay topology was based on the displacement of the decay tracks from the interaction vertex (via their impact parameter, d_0), the separation between the secondary and primary vertices (decay length, L) and the pointing angle of the reconstructed D-meson momentum to the primary vertex. This pointing condition was applied via a selection on the angle $\theta_{\mathrm{pointing}}$ between the direction of the reconstructed momentum of the candidate and the straight line connecting the primary and secondary vertices. The projections of the pointing angle and of the decay length onto the transverse plane ($\theta^{xy}_{\mathrm{pointing}}$ and L^{xy}) were also used. The selection requirements were tuned to provide a large statistical significance for the signal and to keep the selection efficiency as high as possible. The chosen selection values depend on the p_{T} of the D meson and become tighter from peripheral to central collisions. A detailed description of the selection criteria was reported in [32, 35].

In order to further reduce the combinatorial background, pions and kaons were identified using the TPC and TOF detectors. A 3σ compatibility cut was applied to the difference between the measured and expected signals (for pions and kaons) for the TPC $\mathrm{d}E/\mathrm{d}x$ and TOF time-of-flight. Tracks that are not matched with a hit in the TOF detector were identified using only the TPC information. Particle identification (PID) was not applied to the pion track from the D^{*+} decay. This PID selection provides a reduction of the background by a factor of 2–3 at low p_{T} with respect to the case without applying the selection, while having an efficiency of about 95% for the signal.

The raw D-meson yields were obtained from fits to the candidate invariant-mass distributions $M(\mathrm{K}\pi)$ for D^0, $M(\mathrm{K}\pi\pi)$ for D^+, and the mass difference $\Delta M = M(\mathrm{K}\pi\pi) - M(\mathrm{K}\pi)$ for D^{*+}. The D^0 and D^+ candidate invariant-mass distributions were fitted with a function composed of a Gaussian for the signal and an exponential term to describe the background shape. In the 0–10% centrality class, the background in the $M(\mathrm{K}\pi)$ distribution for the interval $1 < p_{\mathrm{T}} < 2\,\mathrm{GeV}/c$ could not be accounted for by an exponential shape and was instead modelled with a fourth-order polynomial function. The ΔM distribution of D^{*+} candidates was fitted with a Gaussian function for the signal and a threshold function multiplied by an exponential for the background: $a\sqrt{\Delta M - m_\pi}\cdot \mathrm{e}^{b(\Delta M - m_\pi)}$.

In the case of D^0 mesons, an additional term was included in the fit function to account for the background from "reflections", i.e. signal candidates that remain in the

JHEP03(2016)081

invariant-mass distribution when the (K, π) mass hypotheses for the two decay tracks are swapped. A study of simulations showed that about 70% of these reflections are rejected by the PID selection, while the residual contribution results in a broad invariant-mass distribution, which can be described using a sum of two Gaussians. In order to account for the contribution of reflections in the data (2–5% at low p_{T}, about 10% at high p_{T}), a template consisting of two Gaussians was included in the fit. The centroids and widths, as well as the ratios of the integrals of these Gaussians to the signal integral, were fixed to the values obtained in the simulations (see also [35]).

In the centrality class 0–10%, the signal extraction was performed in the interval $1<p_{\mathrm{T}}<24\,\mathrm{GeV}/c$ for D^0 mesons, divided in 9 p_{T} bins, and in the interval $3<p_{\mathrm{T}}<36\,\mathrm{GeV}/c$ for D^+ and D^{*+} mesons, divided in 8 p_{T} bins. In the centrality class 30–50%, the signal extraction was possible in the interval $1 < p_{\mathrm{T}} < 16\,\mathrm{GeV}/c$ for D^0 mesons and in the interval $2 < p_{\mathrm{T}} < 16\,\mathrm{GeV}/c$ for D^+ and D^{*+} mesons. Beyond these intervals, the signal extraction was prevented by the low signal-over-background ratio at low p_{T}, and by the low signal yield at high p_{T}. Figure 1 shows the D^0 and D^+ invariant-mass distributions and D^{*+} mass difference distributions in three p_{T} intervals for the centrality class 0–10%. In the interval $16 < p_{\mathrm{T}} < 24\,\mathrm{GeV}/c$ the fit range for the D^0 case is asymmetric. The range was limited to values larger than $1.68\,\mathrm{GeV}/c^2$ because the invariant-mass distribution of (K, π) pairs from D mesons decaying in three or more prongs produces a wide structure below about $1.72\,\mathrm{GeV}/c^2$, which cannot be accounted for by the background terms of the fit function.

Figure 2 shows the background-subtracted D^0 invariant-mass distribution for the interval $1 < p_{\mathrm{T}} < 2\,\mathrm{GeV}/c$ for the 0–10% (left panel) and 30–50% (right panel) centrality classes.

For all three D-meson species, the position of the signal peak was found to be compatible with the world average value and its p_{T}-dependent width with the values observed in the simulation. The statistical significance of the observed signals $\mathrm{S}/\sqrt{\mathrm{S}+\mathrm{B}}$ varies from 3 to 18, while the signal-over-background ratio S/B ranges from 0.01 to 1.8, depending on the meson species, p_{T} interval and centrality class.

3.2 $\mathrm{d}N/\mathrm{d}p_{\mathrm{T}}$ spectra corrections

The D-meson raw yields were corrected in order to obtain the p_{T}-differential yields of prompt D mesons

$$\left.\frac{\mathrm{d}N^{\mathrm{D}}}{\mathrm{d}p_{\mathrm{T}}}\right|_{|y|<0.5} = \frac{f_{\mathrm{prompt}}(p_{\mathrm{T}}) \cdot \frac{1}{2} N_{\mathrm{raw}}^{\mathrm{D}+\overline{\mathrm{D}}}(p_{\mathrm{T}})\Big|_{|y|<y_{\mathrm{fid}}}}{\Delta p_{\mathrm{T}} \cdot \alpha_y \cdot (\mathrm{Acc}\times\epsilon)_{\mathrm{prompt}}(p_{\mathrm{T}}) \cdot \mathrm{BR} \cdot N_{\mathrm{events}}}\,, \tag{3.1}$$

where prompt refers to mesons not coming from weak decays of B hadrons. The raw yields $N_{\mathrm{raw}}^{\mathrm{D}+\overline{\mathrm{D}}}$ were divided by a factor of two to obtain the charge-averaged (particle and antiparticle) yields. To correct for the contribution of B-meson decay feed-down, the raw yields were multiplied by the fraction of promptly produced D mesons, f_{prompt} (discussed in details later in this section). Furthermore, they were divided by the product of prompt D-meson acceptance and efficiency $(\mathrm{Acc}\times\epsilon)_{\mathrm{prompt}}$, by the decay channel branching ratio (BR), by the transverse momentum interval width (Δp_{T}) and by the number of events

JHEP03(2016)081

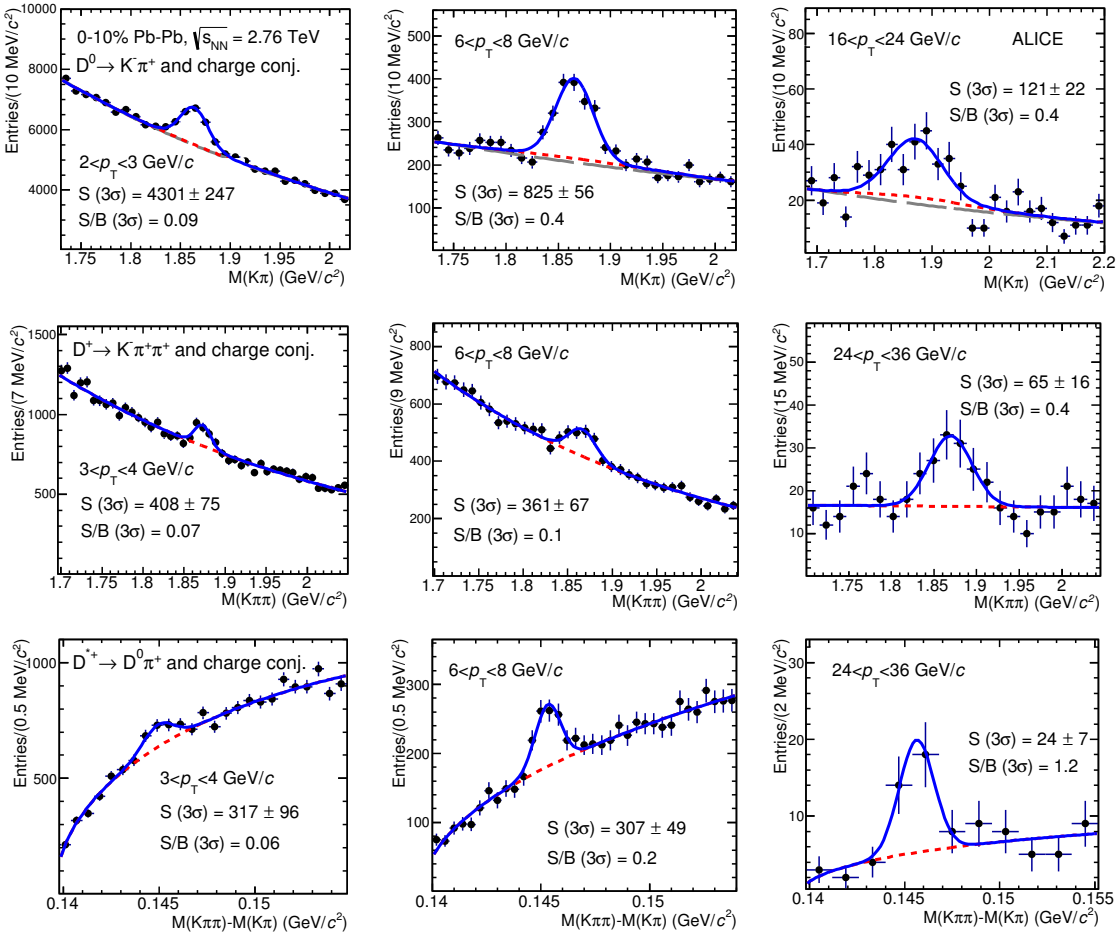

Figure 1. (K, π) (top row) and (K, π, π) (central row) invariant-mass distributions for the centrality class 0–10%. Bottom row: distribution of the mass difference $\Delta M = M(\mathrm{K}\pi\pi) - M(\mathrm{K}\pi)$ for the centrality class 0–10%. The distributions are reported in three p_{T} intervals for each meson (left, middle and right column). The fit functions used to describe the background (dash), the background without signal reflections (only for D^0, long-dash) and the total distribution including the signal (solid) are shown.

(N_{events}). The factor $\alpha_y = y_{\mathrm{fid}}/0.5$ normalises the corrected yields measured in $|y| < y_{\mathrm{fid}}$ to one unit of rapidity $|y| < 0.5$, assuming a uniform rapidity distribution for D mesons in the measured range. This assumption was validated to the 1% level with simulations [45, 46].

The correction for acceptance and efficiency $(\mathrm{Acc} \times \epsilon)_{\mathrm{prompt}}$ was determined using Monte Carlo simulations with a detailed description of the detector and its response, based on the GEANT3 transport package [47]. The simulation was tuned to reproduce the (time-dependent) position and width of the interaction vertex distribution, as well as the number of active read-out channels and the accuracy of the detector calibration. The underlying Pb-Pb events at $\sqrt{s_{\mathrm{NN}}} = 2.76\,\mathrm{TeV}$ were simulated using the HIJING v1.383 generator [48] and D-meson signals were added with the PYTHIA v6.421 generator [49] with Perugia-0 tune [50]. Each simulated PYTHIA pp event contained a $\mathrm{c\bar{c}}$ or $\mathrm{b\bar{b}}$ pair, and D mesons were forced to decay in the hadronic channels of interest for the analysis. Out of all the

JHEP03(2016)081

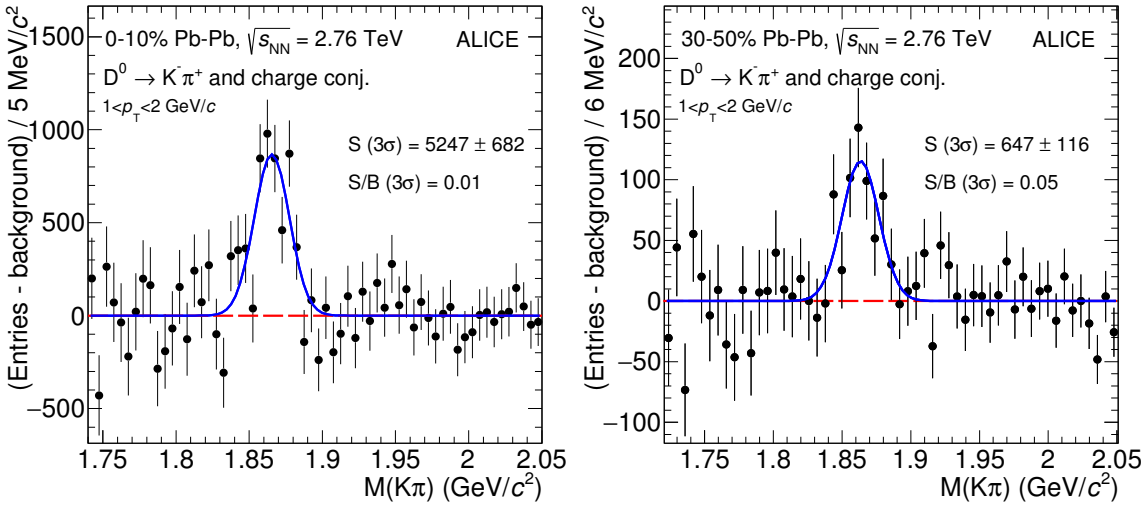

Figure 2. (K, π) invariant-mass distribution for the interval $1 < p_{\mathrm{T}} < 2\,\mathrm{GeV}/c$ for the 0–10% (left) and 30–50% (right) centrality classes, obtained after the subtraction of the background estimated by a fourth-order polynomial function for the most central collisions and an exponential for the 30–50% centrality class. The contribution of reflections is also included in the fit. The fit function used to describe the signal (solid line) is shown.

particles produced in these PYTHIA pp events, only the heavy-flavour decay products were kept and transported through the detector simulation together with the particles produced according to HIJING. In order to minimise the bias on the detector occupancy, the number of D mesons injected into each HIJING event was adjusted according to the Pb-Pb collision centrality. In the most central event class, the p_{T} distribution of D mesons was weighted in order to match the shape measured for the D^0 meson. In the semi-peripheral centrality class, the D-meson p_{T} distribution was weighted so as to match the shape given by fixed-order-next-to-leading-log perturbative QCD calculations (FONLL) [51, 52] multiplied by the $R_{\mathrm{AA}}(p_{\mathrm{T}})$ computed using the BAMPS model [53–55].

The efficiencies were evaluated from simulated events that have the same average charged-particle multiplicity, corresponding to the same detector occupancy, as observed in data in the centrality classes 0–10% and 30–50%. Figure 3 shows the D^0, D^+ and D^{*+} acceptance-times-efficiency (Acc $\times$ ε) for primary and feed-down D mesons with rapidity $|y| < y_{\mathrm{fid}}(p_{\mathrm{T}})$ in the centrality class 0–10%. The efficiencies range from about 0.1% at low p_{T} to 10–30% at high p_{T}, because of the momentum dependence of the D-meson decay length and of the topological selections applied in the different momentum intervals. Also shown in the figure are the (Acc $\times$ ε) values for the case where no PID is applied. The relative difference with respect to the (Acc $\times$ ε) obtained using the PID selection is about 5%, illustrating the high efficiency of the PID criteria. The (Acc $\times$ ε) for D mesons from B-meson decays is larger than for prompt D mesons by a factor of about 1.5, because the decay vertices of the feed-down D mesons are more separated from the primary vertex and are, therefore, more efficiently selected by the analysis cuts.

JHEP03(2016)081

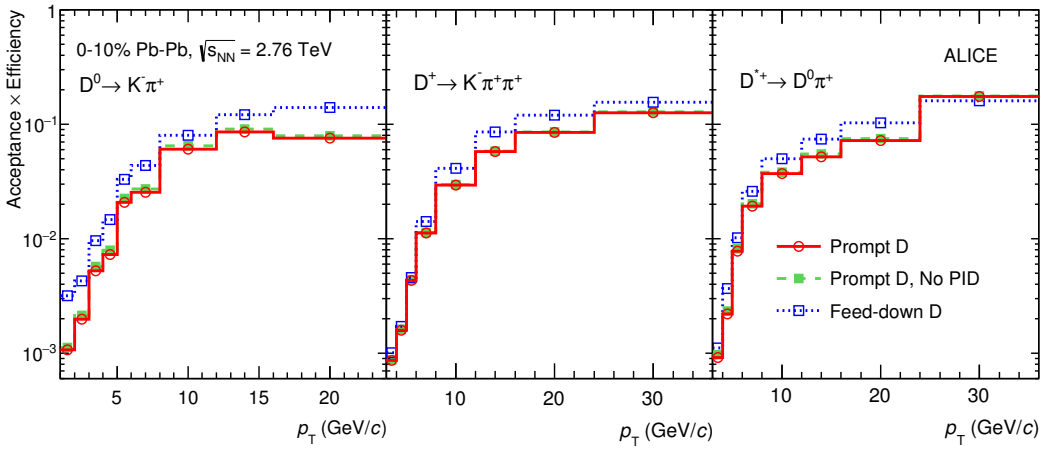

Figure 3. Product of acceptance and efficiency for D mesons in Pb-Pb collisions for the 0–10% centrality class. The rapidity interval is $|y| < y_{\rm fid}$ (see section 3.1). The values for prompt (solid lines) and feed-down (dotted lines) D mesons are shown. Also displayed, for comparison, are the values for prompt D mesons without PID selection (dashed lines).

The $f_{\rm prompt}$ factor was obtained, following the procedure introduced in [32], as

$$f_{\rm prompt} = 1 - \frac{N_{\rm raw}^{\rm D+\overline{D}\,feed\text{-}down}}{N_{\rm raw}^{\rm D+\overline{D}}} = 1 - R_{\rm AA}^{\rm feed\text{-}down} \cdot \langle T_{\rm AA} \rangle \cdot \left(\frac{{\rm d}\sigma}{{\rm d}p_{\rm T}} \right)^{\rm FONLL,\,EvtGen}_{\rm feed\text{-}down,|y|<0.5} \cdot \frac{\Delta p_{\rm T} \cdot \alpha_y \cdot ({\rm Acc} \times \epsilon)_{\rm feed\text{-}down} \cdot {\rm BR} \cdot N_{\rm events}}{\frac{1}{2} N_{\rm raw}^{\rm D+\overline{D}}}. \tag{3.2}$$

In this expression, the symbols denoting the $p_{\rm T}$ dependence have been omitted for brevity, $N_{\rm raw}^{\rm D+\overline{D}}$ is the measured raw yields and $N_{\rm raw}^{\rm D+\overline{D}\,feed\text{-}down}$ is the estimated raw yields of D mesons from B-meson decays. In detail, the B-meson production cross section in pp collisions at $\sqrt{s} = 2.76$ TeV, estimated with FONLL calculations [56], was folded with the B $\to$ D + X decay kinematics using the EvtGen package [57] and multiplied by $\langle T_{\rm AA} \rangle$ in each centrality class, by the (Acc $\times$ ε) for feed-down D mesons, and by the other factors introduced in eq. (3.1). In addition, the nuclear modification factor of D mesons from B-meson decays was accounted for. The comparison of the $R_{\rm AA}$ of prompt D mesons ($R_{\rm AA}^{\rm prompt}$) [58] with that of J/ψ from B-meson decays [59] measured in the CMS experiment indicates that charmed hadrons are more suppressed than beauty hadrons. The value $R_{\rm AA}^{\rm feed\text{-}down} = 2 \cdot R_{\rm AA}^{\rm prompt}$ was used to compute the correction, and the variation over the range $1 < R_{\rm AA}^{\rm feed\text{-}down}/R_{\rm AA}^{\rm prompt} < 3$ was considered for the evaluation of the systematic uncertainties, in order to take into account possible centrality and $p_{\rm T}$ dependences. Assuming $R_{\rm AA}^{\rm feed\text{-}down} = 2 \cdot R_{\rm AA}^{\rm prompt}$, the resulting $f_{\rm prompt}$ ranges from about 0.65 to 0.85, depending on the D-meson species and on the $p_{\rm T}$ interval.

JHEP03(2016)081

3.3 Proton-proton reference for $R_{\rm AA}$

The $p_{\rm T}$-differential cross section of prompt D mesons with $|y| < 0.5$ in pp collisions at $\sqrt{s} = 2.76\,\text{TeV}$, used as reference for the nuclear modification factor, was obtained as follows:

- in the interval $2 < p_{\rm T} < 16\,(24)\,\text{GeV}/c$ for $\rm D^0$ ($\rm D^+$ and $\rm D^{*+}$), the measurement at $\sqrt{s} = 7\,\text{TeV}$ [45] scaled to $\sqrt{s} = 2.76\,\text{TeV}$ with FONLL calculations [56] was used;
- in the interval $1 < p_{\rm T} < 2\,\text{GeV}/c$ for $\rm D^0$, an average of the aforementioned $\sqrt{s} = 7\,\text{TeV}$ scaled measurement and of the measurement at $\sqrt{s} = 2.76\,\text{TeV}$ [60] was used;
- in the interval $16\,(24) < p_{\rm T} < 24\,(36)\,\text{GeV}/c$ for $\rm D^0$ ($\rm D^+$ and $\rm D^{*+}$), where their cross sections were not measured in pp collisions, the FONLL calculation at $\sqrt{s} = 2.76\,\text{TeV}$ [56] was used as a reference, after scaling it to match the central value of the data at lower $p_{\rm T}$.

The $p_{\rm T}$-dependent scaling factor from $\sqrt{s} = 7\,\text{TeV}$ to $\sqrt{s} = 2.76\,\text{TeV}$ was determined with FONLL calculations and its uncertainties were determined by varying the parameters (charm-quark mass, factorisation and renormalisation scales) as described in [61]. The uncertainties on the scaling factor range from $^{+57}_{-11}\%$ for $1 < p_{\rm T} < 2\,\text{GeV}/c$ to about $\pm 5\%$ for $p_{\rm T} > 10\,\text{GeV}/c$. The result of the scaling of the $\sqrt{s} = 7\,\text{TeV}$ $p_{\rm T}$-differential cross sections to $\sqrt{s} = 2.76\,\text{TeV}$ was validated with measurements from a smaller data sample in pp collisions at $\sqrt{s} = 2.76\,\text{TeV}$ [60]. These measurements cover a reduced $p_{\rm T}$ interval with a statistical uncertainty of 20–25% and therefore they were not used as a pp reference for $p_{\rm T} > 2\,\text{GeV}/c$.

For the lowest $p_{\rm T}$ interval for the $\rm D^0$ meson, the two references (obtained from the measurement in pp collisions at $\sqrt{s} = 2.76\,\text{TeV}$ and from the $\sqrt{s} = 7\,\text{TeV}$ scaled measurement) have comparable uncertainties. Therefore, in this interval, the two values were averaged using the inverse of the squared relative uncertainties as weights. In particular, the statistical uncertainties and the uncorrelated part of the systematic uncertainties, i.e. the systematic uncertainty from data analysis (yield extraction, efficiency corrections) and the scaling uncertainty, were used in the weight. The uncertainties on the feed-down subtraction were considered as fully correlated among the two measurements, and were propagated linearly.

The cross section measurements for D mesons in pp collisions at $\sqrt{s} = 7\,\text{TeV}$ are limited to $p_{\rm T} \leq 16\,\text{GeV}/c$ for $\rm D^0$ and to $p_{\rm T} \leq 24\,\text{GeV}/c$ for $\rm D^+$ and $\rm D^{*+}$. Beyond these limits the pp reference was obtained using the cross section from the FONLL calculation at $\sqrt{s} = 2.76\,\text{TeV}$ [56]. Since the central value of the FONLL calculation underestimates the measurement for $p_{\rm T} > 5\,\text{GeV}/c$ at both $\sqrt{s} = 2.76\,\text{TeV}$ and $\sqrt{s} = 7\,\text{TeV}$ [45, 60], the FONLL cross section was multiplied by a scaling factor (κ)

$$\frac{\mathrm{d}\sigma}{\mathrm{d}p_{\rm T}} = \kappa \cdot \left(\frac{\mathrm{d}\sigma}{\mathrm{d}p_{\rm T}}\right)^{\rm FONLL}_{\sqrt{s}=2.76\,\text{TeV},\,|y|<0.5} . \tag{3.3}$$

JHEP03(2016)081

The factor κ was determined by fitting with a constant the data-to-theory ratio at $\sqrt{s} = 7\,\text{TeV}$ in the interval $5 < p_{\text{T}} < 16\,\text{GeV}/c$. Since the measurements at $\sqrt{s} = 2.76\,\text{TeV}$ are less precise, they do not constrain further the scaling factor. Depending on the D-meson species, the factor κ ranges from 1.4 to 1.5, for the central values of the FONLL calculation parameters [56]. The statistical uncertainty of the extrapolated cross section was determined by propagating the statistical uncertainties of the measurement in the determination of κ and it amounts to about 5%. The systematic uncertainties were evaluated under the conservative assumption that the systematic uncertainties of the measurement are fully correlated over p_{T}, i.e. by repeating the calculation of κ after shifting all data points consistently within their systematic uncertainties. In addition, the calculation in eq. (3.3) was performed considering the FONLL cross sections obtained from combinations of the renormalisation and factorisation scales with values $(0.5, 1, 2) \cdot \sqrt{m_{\text{c}}^2 + p_{\text{T,c}}^2}$ [56], as well as the upper and lower limits of their envelope.[1] This resulted in a total systematic uncertainty on the p_{T}-extrapolated cross section of about $^{+50}_{-35}$%.

4 Systematic uncertainties

4.1 Systematic uncertainties on the D-meson p_{T} spectra

The systematic uncertainties were estimated as a function of transverse momentum for the two centrality classes. Table 2 lists the uncertainties for three p_{T} intervals for each meson species.

The systematic uncertainty on the raw yield extraction was evaluated by repeating the fit of the invariant-mass distributions while varying the fit range; by fixing the mean and sigma of the Gaussian term to the world-average value and the expectations from Monte Carlo simulations, respectively; and by using different fit functions for the background. Specifically, first- and second-order polynomials were used for D^0 and D^+, and a power law multiplied by an exponential or a threshold function for D^{*+}. A method based on bin counting of the signal after background subtraction was also used. This method does not assume any particular shape for the invariant-mass distribution of the signal. The estimated uncertainties depend on the centrality class and on the p_{T} interval, ranging from 5% to 15% for D^0, 8% to 10% for D^+ and 5% to 10% for D^{*+}, typically with larger values in the lowest and highest p_{T} intervals.

For D^0 mesons, the systematic uncertainty due to signal reflections in the invariant-mass distribution was estimated by changing by ±50% the ratio of the integral of the reflections over the integral of the signal (obtained from the simulation) used in the invariant-mass fit with the reflections template. In addition, the shape of the template was varied using a polynomial parameterisation (of third or sixth order) of the simulated distribution, instead of a double-Gaussian parameterisation. A test was carried out using, in the fit, a template histogram of the reflections obtained directly from the simulation, rather than a functional form. The variation observed in the raw yields, ranging from 3% to 7% from low

[1] Where m_{c} and $p_{\text{T,c}}$ are respectively the mass and the transverse momentum of the charm quark considered in the calculations.

JHEP03(2016)081

Particle	D^0			D^+			D^{*+}		
0–10% centrality class									
p_T interval (GeV/c)	1–2	6–8	16–24	3–4	6–8	24–36	3–4	6–8	24–36
Yield extraction	15%	5%	15%	10%	8%	8%	12%	5%	10%
Tracking efficiency	10%	10%	10%	15%	15%	15%	15%	15%	15%
Selection cuts	15%	5%	5%	10%	10%	10%	10%	10%	10%
PID efficiency	5%	5%	5%	5%	5%	5%	5%	5%	5%
MC p_T shape	15%	1%	1%	6%	1%	1%	4%	1%	1%
FONLL feed-down corr.	$^{+5}_{-45}$%	$^{+8}_{-13}$%	$^{+10}_{-16}$%	$^{+4}_{-12}$%	$^{+6}_{-11}$%	$^{+8}_{-14}$%	$^{+3}_{-12}$%	$^{+4}_{-7}$%	$^{+3}_{-8}$%
$R_{AA}^{\text{feed-down}}/R_{AA}^{\text{prompt}}$ (eq. (3.2))	$^{+5}_{-5}$%	$^{+11}_{-10}$%	$^{+16}_{-13}$%	$^{+6}_{-5}$%	$^{+9}_{-7}$%	$^{+14}_{-11}$%	$^{+4}_{-4}$%	$^{+6}_{-6}$%	$^{+6}_{-6}$%
BR		1.3%			2.1%			1.5%	
Centrality class definition		< 1%			< 1%			< 1%	
30–50% centrality class									
p_T interval (GeV/c)	1–2	6–8	12–16	2–3	6–8	12–16	2–3	6–8	12–16
Yield extraction	10%	8%	8%	10%	10%	12%	12%	8%	5%
Tracking efficiency	10%	10%	10%	15%	15%	15%	15%	15%	15%
Selection cuts	10%	10%	15%	10%	10%	15%	15%	10%	5%
PID efficiency	5%	5%	5%	5%	5%	5%	5%	5%	5%
MC p_T shape	5%	1%	3%	10%	2%	2%	10%	1%	1%
FONLL feed-down corr.	$^{+5}_{-45}$%	$^{+7}_{-12}$%	$^{+8}_{-11}$%	$^{+6}_{-21}$%	$^{+6}_{-12}$%	$^{+11}_{-13}$%	$^{+3}_{-19}$%	$^{+5}_{-8}$%	$^{+4}_{-8}$%
$R_{AA}^{\text{feed-down}}/R_{AA}^{\text{prompt}}$ (eq. (3.2))	$^{+6}_{-5}$%	$^{+11}_{-9}$%	$^{+14}_{-11}$%	$^{+7}_{-6}$%	$^{+9}_{-8}$%	$^{+16}_{-12}$%	$^{+4}_{-4}$%	$^{+7}_{-6}$%	$^{+6}_{-6}$%
BR		1.3%			2.1%			1.5%	
Centrality class definition		2%			2%			2%	

Table 2. Relative systematic uncertainties on the prompt D-meson production yields in Pb-Pb collisions for three selected p_T intervals, in the two centrality classes.

to high p_T, was added in quadrature as an independent contribution to the yield extraction systematic uncertainty.

The systematic uncertainty on the tracking efficiency was estimated by comparing the probability to match the TPC tracks to the ITS hits in data and simulation, and by varying the track quality selection criteria (for example, the minimum number of associated hits in the TPC and in the ITS, and the maximum χ^2/ndf of the momentum fit). The efficiency of the track matching and the association of hits in the silicon pixel layers was found to be well reproduced by the simulation with maximal deviations on the level of 5% in the p_T range relevant for this analysis (0.5–25 GeV/c) [37]. The effect of mis-associating ITS hits to tracks was studied using simulations. The mis-association probability is about 5%, for central collisions, in the transverse momentum interval $1 < p_T < 3$ GeV/c and drops rapidly to zero at larger p_T. It was verified that the signal selection efficiencies are the same for D mesons with and without wrong hit associations. The total systematic uncertainty

JHEP03(2016)081

on the track reconstruction procedure amounts to 5% for single tracks, which results in a 10% uncertainty for D^0 mesons (two-tracks decay) and 15% for D^+ and D^{*+} mesons (three-tracks decay).

The uncertainty on the D-meson selection efficiency reflects a possible non-exact description of the D-meson kinematic properties and of the detector resolutions and alignments in the simulation. This effect was estimated by repeating the analysis with different values of the selection cuts, significantly modifying the efficiencies, raw yield and background values. As expected, larger deviations in the corrected yields were observed at low p_{T}, where the efficiencies are low and vary steeply with p_{T}, because of the tighter selections. Due to this, the systematic uncertainties are slightly larger in these p_{T} intervals. The assigned systematic uncertainty varies from 5% to 15% for D^0, equals 10% for D^+, and varies from 10% to 15% for D^{*+}.

A 5% systematic uncertainty related to the PID selection was evaluated by comparing the ratio of the corrected yields extracted with and without particle identification.

The uncertainty on the efficiencies arising from the difference between the real and simulated D-meson transverse momentum distributions depends on the width of the p_{T} intervals and on the variation of the efficiencies within them. This uncertainty also includes the effect of the p_{T} dependence of the nuclear modification factor. As explained in section 3.2, for the centrality class 0–10%, the D-meson transverse momentum distribution from the PYTHIA simulation was re-weighted in order to reproduce the D^0 spectrum shape observed in data, while for the 30–50% centrality class, the weights were defined in order to match the p_{T} distributions from FONLL calculations multiplied by the R_{AA} from the BAMPS model. A systematic uncertainty was estimated by using two alternative D-meson p_{T} distributions in both centrality classes: i) FONLL p_{T} distributions, ii) FONLL p_{T} distributions multiplied by R_{AA} from the BAMPS model. In addition, for the most central events, a different parameterisation of the measured p_{T} spectrum was used. The resulting uncertainties decrease with increasing p_{T}, varying from 5–6% to 1% in the interval $2 < p_{\mathrm{T}} < 36\,\mathrm{GeV}/c$. For D^0 mesons, efficiencies increase by more than a factor five within the interval $1 < p_{\mathrm{T}} < 2\,\mathrm{GeV}/c$ in the most central collisions. As a consequence, a larger uncertainty of 15% resulted from a detailed study of the stability of the corrected yields when changing the p_{T} spectrum in the simulation.

The systematic uncertainty on the subtraction of feed-down from B decays (i.e. the calculation of the f_{prompt} fraction) was estimated i) by varying the p_{T}-differential feed-down D-meson cross section from the FONLL calculation within the theoretical uncertainties, ii) by varying the hypothesis on the ratio of the prompt and feed-down D-meson R_{AA} in the range $1 < R_{\mathrm{AA}}^{\text{feed-down}}/R_{\mathrm{AA}}^{\text{prompt}} < 3$, and iii) by applying an alternative method to compute f_{prompt}. This second method is based on the ratio of charm and beauty FONLL cross sections, instead of the absolute beauty cross section. The procedure is the same used for previous measurements of D-meson production with ALICE [32, 35, 45]. The resulting uncertainty ranges between $^{+5}_{-45}$% at low p_{T} and $^{+3}_{-8}$% at high p_{T} for the 0–10% centrality class, and between $^{+5}_{-45}$% at low p_{T} and $^{+4}_{-8}$% at high p_{T} for the 30–50% centrality class. The uncertainty from the variation of the feed-down D-meson R_{AA} hypothesis ranges from 6 to 16%, as shown in figure 4, where the relative variation of the prompt D^0 yield is shown as a function of the hypothesis on $R_{\mathrm{AA}}^{\text{feed-down}}/R_{\mathrm{AA}}^{\text{prompt}}$ for four p_{T} intervals.

JHEP03(2016)081

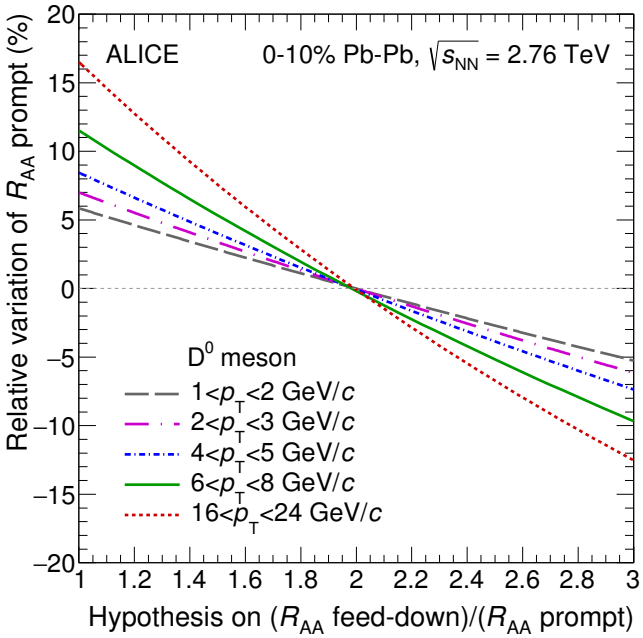

Figure 4. Relative variation of the prompt D^0 yields as a function of the hypothesis on $R_{AA}^{\text{feed-down}}/R_{AA}^{\text{prompt}}$ for the B-meson feed-down subtraction.

The uncertainties on the branching ratios were also considered [44] as well as the contribution due to the 1.1% uncertainty on the fraction of the hadronic cross section used in the Glauber fit to determine the centrality classes [39]. The latter was estimated from the variation of the D-meson dN/dp_T when the limits of the centrality classes are shifted by ±1.1% (e.g. shifted from 30–50% to 30.3–50.6% and 29.7–49.5%) [32]. The resulting uncertainty, common to all p_T intervals, is smaller than 1% for the 0–10% centrality class and about 2% for the 30–50% centrality class.

4.2 Systematic uncertainties on R_{AA}

The systematic uncertainties on the R_{AA} measurement include those on the D-meson corrected yields, those on the proton-proton cross section reference, and the uncertainties on the average nuclear overlap function.

The systematic uncertainties on the D-meson corrected yields are obtained considering as uncorrelated the different contributions described in the previous section.

The uncertainty on the pp reference used for the calculation of R_{AA} has two contributions. The first is the systematic uncertainty on the measured p_T-differential D-meson cross section at $\sqrt{s} = 7$ TeV. This uncertainty is about 25% at the lowest p_T and 17% at the highest p_T for D^0 mesons, excluding the uncertainty for feed-down corrections, and few percent larger for D^+ and D^{*+} mesons [45]. The systematic uncertainty on the feed-down subtraction deriving from the variation of the parameters of the FONLL calculation and from the use of the alternative method to compute f_{prompt} was considered to be correlated in the Pb-Pb and pp measurements. These variations were carried out simultaneously for

JHEP03(2016)081

Particle	D^0			D^+			D^{*+}		
0–10% centrality class									
p_T interval (GeV/c)	1–2	6–8	16–24	3–4	6–8	24–36	3–4	6–8	24–36
dN_{Pb-Pb}/dp_T (excl. feed-down)	28%	14%	22%	22%	20%	22%	24%	20%	21%
dN_{pp}/dp_T (excl. feed-down)	21%*	16%	17%	20%	19%	20%	17%	17%	18%
$\sqrt{s}$ – scaling of the pp ref.	$^{+\ 6}_{-30}$%*	$^{+\ 6}_{-10}$%	—	$^{+\ 8}_{-19}$%	$^{+\ 6}_{-10}$%	—	$^{+\ 9}_{-20}$%	$^{+\ 6}_{-10}$%	–
High-p_T extrapolation	—	—	$^{+34}_{-51}$%	—	—	$^{+37}_{-56}$%	—	—	$^{+34}_{-53}$%
FONLL feed-down corr.	$^{+\ 1}_{-\ 4}$%	$^{+\ 2}_{-\ 4}$%	$^{+10}_{-16}$%	$^{+\ 2}_{-\ 1}$%	$^{+\ 1}_{-\ 2}$%	$^{+\ 8}_{-14}$%	$^{+\ 1}_{-\ 4}$%	$^{+\ 2}_{-\ 4}$%	$^{+\ 3}_{-\ 8}$%
$R_{AA}^{\text{feed-down}}/R_{AA}^{\text{prompt}}$ (eq. (3.2))	$^{+12}_{-\ 9}$%	$^{+14}_{-11}$%	$^{+19}_{-13}$%	$^{+\ 8}_{-\ 7}$%	$^{+12}_{-\ 9}$%	$^{+16}_{-12}$%	$^{+\ 6}_{-\ 6}$%	$^{+\ 8}_{-\ 7}$%	$^{+\ 8}_{-\ 7}$%
Normalisation		4.8%			4.8%			4.8%	
30–50% centrality class									
p_T interval (GeV/c)	1–2	6–8	12–16	2–3	6–8	12–16	2–3	6–8	12–16
dN_{Pb-Pb}/dp_T (excl. feed-down)	20%	20%	22%	25%	21%	22%	29%	19%	18%
dN_{pp}/dp_T (excl. feed-down)	21%*	16%	17%	20%	19%	20%	17%	17%	18%
$\sqrt{s}$ – scaling of the pp ref.	$^{+\ 6}_{-30}$%*	$^{+\ 6}_{-10}$%	$^{+5}_{-6}$%	$^{+\ 8}_{-19}$%	$^{+\ 6}_{-10}$%	$^{+5}_{-6}$%	$^{+\ 9}_{-20}$%	$^{+\ 6}_{-10}$%	$^{+5}_{-6}$%
FONLL feed-down corr.	$^{+\ 1}_{-\ 5}$%	$^{+\ 2}_{-\ 3}$%	$^{+\ 3}_{-\ 4}$%	$^{+\ 1}_{-\ 2}$%	$^{+\ 1}_{-\ 3}$%	$^{+\ 3}_{-\ 4}$%	$^{+\ 1}_{-\ 2}$%	$^{+\ 3}_{-\ 5}$%	$^{+\ 2}_{-\ 3}$%
$R_{AA}^{\text{feed-down}}/R_{AA}^{\text{prompt}}$ (eq. (3.2))	$^{+12}_{-\ 9}$%	$^{+14}_{-11}$%	$^{+15}_{-11}$%	$^{+\ 9}_{-\ 7}$%	$^{+13}_{-10}$%	$^{+17}_{-13}$%	$^{+\ 7}_{-\ 6}$%	$^{+10}_{-\ 8}$%	$^{+\ 9}_{-\ 8}$%
Normalisation		6.2%			6.2%			6.2%	

Table 3. Relative systematic uncertainties on the prompt D-meson R_{AA} for three p_T intervals, in the two centrality classes. Uncertainties marked with a * were obtained as the average of the measurement at $\sqrt{s} = 2.76$ TeV and the measurement at $\sqrt{s} = 7$ TeV, scaled using FONLL [56], as described in section 3.3.

the numerator and denominator of R_{AA}, so only the residual effect was attributed as a systematic uncertainty. Therefore, the variation of the value of $R_{AA}^{\text{feed-down}}/R_{AA}^{\text{prompt}}$ between 1 and 3 is the main contribution to the feed-down uncertainty on R_{AA}.

The second contribution to the pp reference uncertainty is the scaling to $\sqrt{s}=2.76$ TeV. It ranges from $^{+27}_{-10}$% in the interval $2 < p_T < 3$ GeV/c to about 5% for $p_T > 10$ GeV/c [61]. Note that the upper/lower uncertainties are reversed when considering R_{AA}, where the pp reference is in the denominator. In the interval 1–2 GeV/c, this scaling uncertainty is much larger ($^{+57}_{-11}$%), but its impact on the pp reference was reduced by about a factor of two by using a weighted average of the cross section scaled from 7 TeV and the measured cross section at 2.76 TeV (see section 3.3).

The extrapolation of the pp reference to the intervals $16 < p_T < 24$ GeV/c for D^0 mesons and $24 < p_T < 36$ GeV/c for D^+ and D^{*+} mesons resulted in a total systematic uncertainty of about $^{+35}_{-50}$%, as described in section 3.3.

The uncertainties on R_{AA} are listed in table 3. The uncertainties on the normalisation are the quadratic sum of the pp normalisation uncertainty (3.5%) and the uncertainty on $\langle T_{AA} \rangle$, which is 3.2% and 4.7% in the 0–10% and 30–50% centrality classes, respectively.

All the uncertainties described in this section that result from detector effects are considered to be largely correlated over transverse momentum, with the exception of the

JHEP03(2016)081

yield extraction uncertainty that depends on the S/B in each p_{T} interval. The uncertainties related to the feed-down assumptions and to the $\sqrt{s}$-scaled pp reference are fully correlated over p_{T}, with the exception of that for the hypothesis on the ratio of the prompt and feed-down D-meson R_{AA} that might not be constant as a function of p_{T}.

5 Results and discussion

5.1 D-meson p_{T} spectra and R_{AA}

The transverse momentum distributions $\mathrm{d}N/\mathrm{d}p_{\mathrm{T}}$ of prompt D^0, D^+ and D^{*+} mesons are shown in figures 5a, 5b and 5c for the 10% most central Pb-Pb collisions. The results are presented in the interval $1 < p_{\mathrm{T}} < 24\,\mathrm{GeV}/c$ for the D^0 mesons and $3 < p_{\mathrm{T}} < 36\,\mathrm{GeV}/c$ for D^+ and D^{*+} mesons. They are compared to the corresponding pp cross section reference multiplied by $\langle T_{\mathrm{AA}} \rangle$. The vertical bars represent the statistical uncertainties, the empty boxes the systematic uncertainties from the data analysis, and the shaded boxes the systematic uncertainty due to the subtraction of the feed-down from B-hadron decays. Uncertainties on the pp cross section normalisation and on the branching ratios are quoted separately. A clear suppression of the D-meson yields is observed at intermediate ($3 < p_{\mathrm{T}} < 8\,\mathrm{GeV}/c$) and high transverse momenta ($p_{\mathrm{T}} > 8\,\mathrm{GeV}/c$) in central Pb-Pb collisions as compared to the binary-scaled pp reference. In figure 5d the transverse momentum distributions of prompt D^0, D^+ and D^{*+} mesons in the 10% most central collisions are compared to each other. The $\mathrm{d}N/\mathrm{d}p_{\mathrm{T}}$ values of D^{*+} mesons are scaled by a factor of five for visibility.

The D-meson $\mathrm{d}N/\mathrm{d}p_{\mathrm{T}}$ distributions measured in the 30–50% centrality class are shown in figure 6. Also for this centrality class, a clear suppression of the D-meson yields as compared to the expectation based on binary scaling of the pp yields is observed for $p_{\mathrm{T}} > 3\,\mathrm{GeV}/c$. In figure 6d, the $\mathrm{d}N/\mathrm{d}p_{\mathrm{T}}$ of prompt D^0, D^+ and D^{*+} (the latter scaled by a factor of five) are compared to each other.

Figure 7 shows the p_{T}-dependent ratios of $\mathrm{D}^+/\mathrm{D}^0$ and $\mathrm{D}^{*+}/\mathrm{D}^0$ for central Pb-Pb collisions. They are found to be compatible within uncertainties with those measured in pp collisions at $\sqrt{s} = 7\,\mathrm{TeV}$ [62]. Similar results were also found for the 30–50% centrality class. Therefore, no modification of the relative abundances of these three D-meson species is observed within the current uncertainties in central and semi-central Pb-Pb collisions relative to the pp ones at LHC energies.

The R_{AA} of prompt D^0, D^+ and D^{*+} mesons is shown in figure 8 for the 0–10% (left panel) and 30–50% (right panel) centrality classes. The statistical uncertainties, represented by the vertical error bars, range from 10% in the intermediate p_{T} range up to about 25–30% in the lowest and highest p_{T} intervals, for the 10% most central collisions. The statistical uncertainty on the reference measurement at $\sqrt{s} = 7\,\mathrm{TeV}$ dominates this uncertainty in the interval $2 < p_{\mathrm{T}} < 16\,\mathrm{GeV}/c$. For the 30–50% centrality class, the statistical uncertainties at low and intermediate p_{T} are similar in magnitude to those of central collisions and are about 20% in the interval $12 < p_{\mathrm{T}} < 16\,\mathrm{GeV}/c$. The total p_{T}-dependent systematic uncertainties, described in the previous section, are shown as empty boxes. The normalisation uncertainty is represented by a filled box at $R_{\mathrm{AA}} = 1$. The nuclear modification factors of the three D-meson species are compatible within statistical uncertainties

JHEP03(2016)081

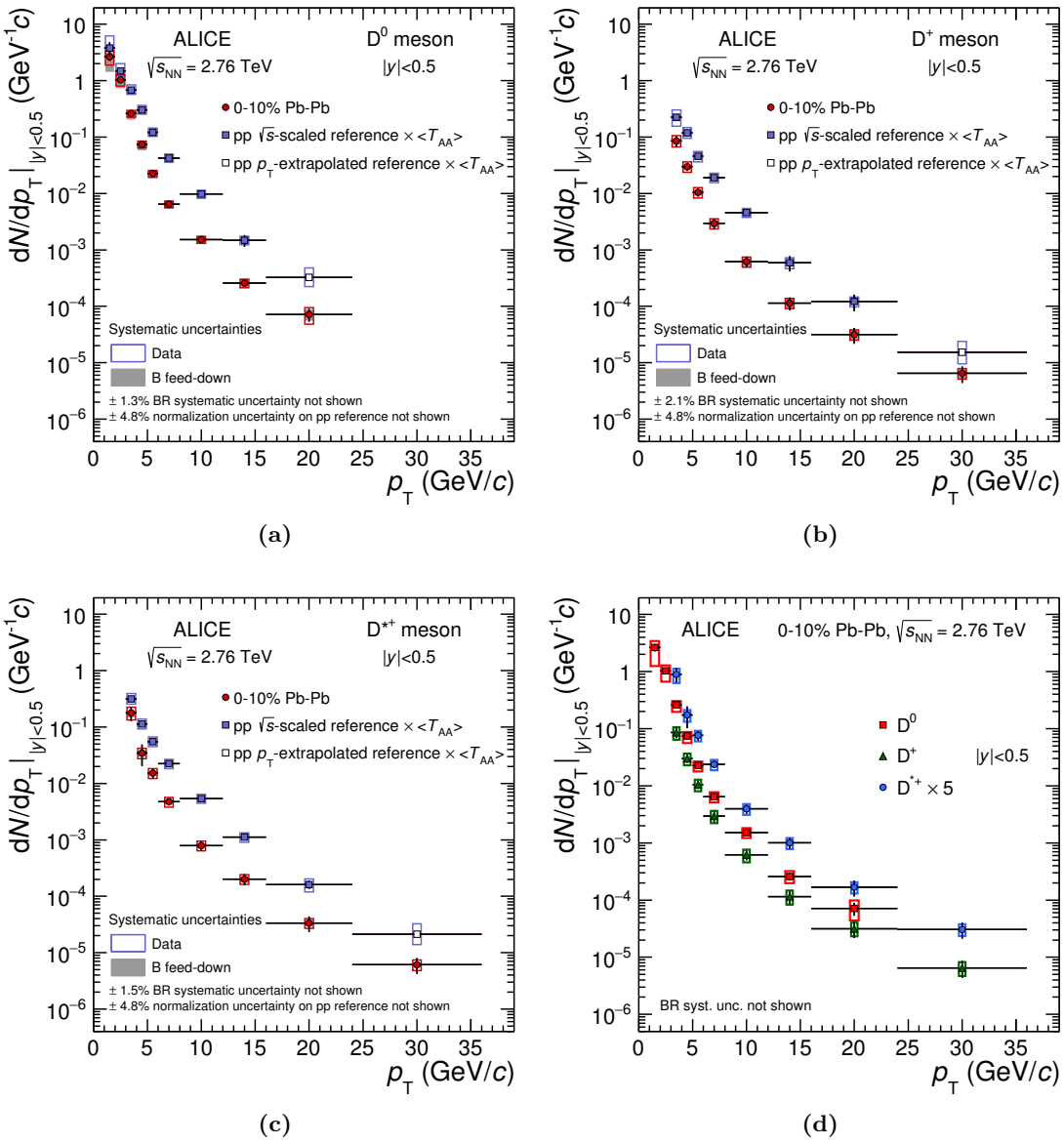

Figure 5. Transverse momentum distributions $\mathrm{d}N/\mathrm{d}p_{\mathrm{T}}$ of prompt D^0 (a), D^+ (b) and D^{*+} (c) mesons in the 0–10% centrality class in Pb-Pb collisions at $\sqrt{s_{\mathrm{NN}}} = 2.76\,\mathrm{TeV}$. The pp reference distributions $\langle T_{\mathrm{AA}} \rangle\ \mathrm{d}\sigma/\mathrm{d}p_{\mathrm{T}}$ are shown as well. Statistical uncertainties (bars) and systematic uncertainties from data analysis (empty boxes) and from feed-down subtraction (shaded boxes) are shown. Horizontal bars represent bin widths, symbols are placed at the centre of the bin. The $\mathrm{d}N/\mathrm{d}p_{\mathrm{T}}$ distributions of the three D-meson species in the 10% most central Pb-Pb collisions are compared to each other in panel (d), where the D^{*+} production yields are scaled by a factor of five for visibility.

for both centrality classes. For the 10% most central collisions, the measured R_{AA} shows a suppression that is maximal at around $p_{\mathrm{T}} = 10\,\mathrm{GeV}/c$, where a reduction of the yields by a factor of 5–6 with respect to the binary-scaled pp reference is observed. The suppression decreases with decreasing p_{T} for $p_{\mathrm{T}} < 10\,\mathrm{GeV}/c$, and it is of the order of a factor of 3 in

JHEP03(2016)081

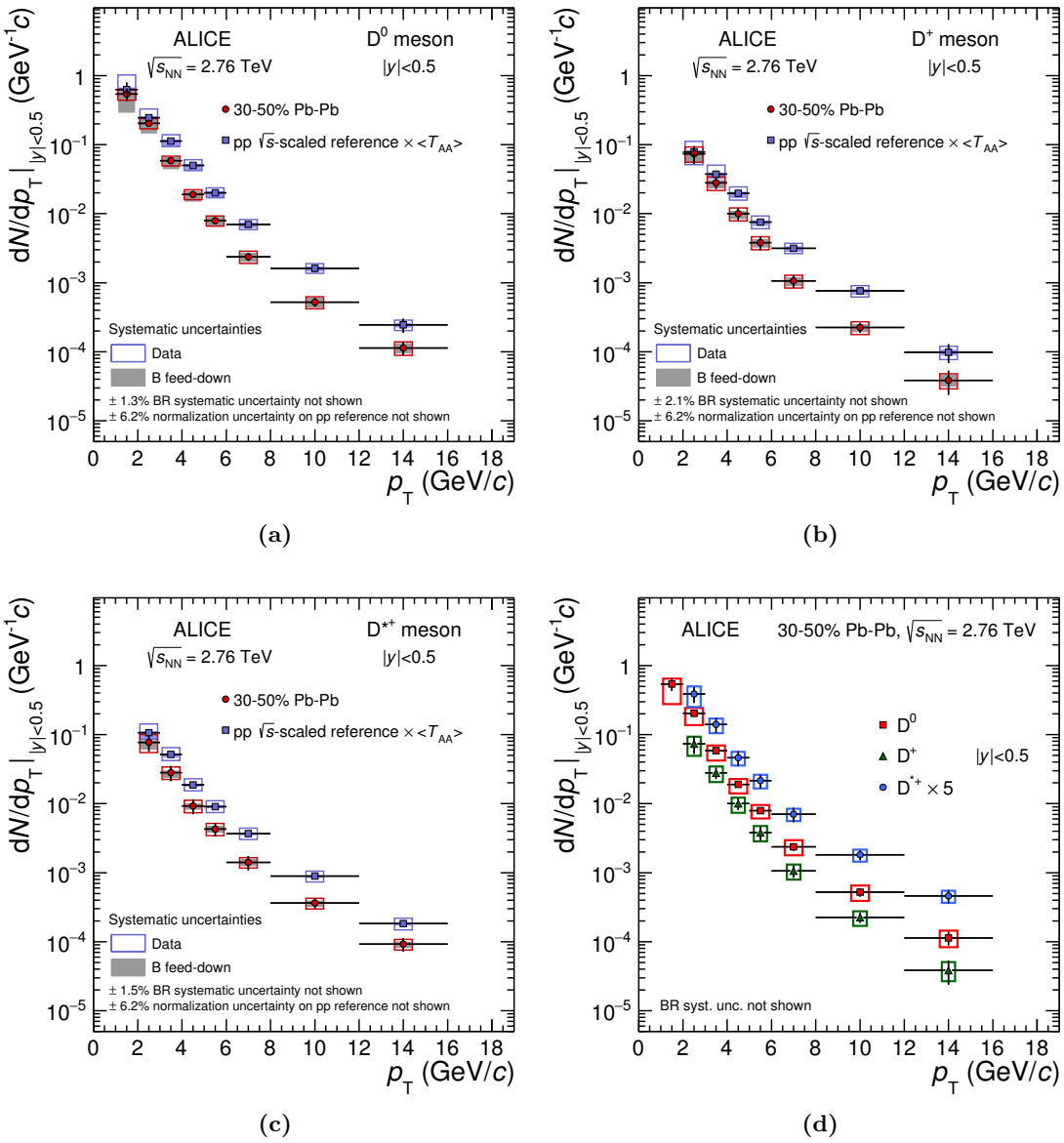

Figure 6. Transverse momentum distributions $\mathrm{d}N/\mathrm{d}p_\mathrm{T}$ of prompt D^0 (a), D^+ (b) and D^{*+} (c) mesons in the 30–50% centrality class in Pb-Pb collisions at $\sqrt{s_\mathrm{NN}} = 2.76\,\mathrm{TeV}$. The pp reference distributions $\langle T_\mathrm{AA}\rangle\,\mathrm{d}\sigma/\mathrm{d}p_\mathrm{T}$ are shown as well. Statistical uncertainties (bars) and systematic uncertainties from data analysis (empty boxes) and from feed-down subtraction (shaded boxes) are shown. Horizontal bars represent bin widths, symbols are placed at the centre of the bin. The $\mathrm{d}N/\mathrm{d}p_\mathrm{T}$ distributions of the three D-meson species in Pb-Pb collisions in the 30–50% centrality class are compared to each other in panel (d), where the D^{*+} production yields are scaled by a factor of five for visibility.

the interval $3 < p_\mathrm{T} < 4\,\mathrm{GeV}/c$, while the R_AA ranges from about 0.35 to 1 in the first two p_T intervals. For $p_\mathrm{T} > 10\,\mathrm{GeV}/c$, the suppression appears to decrease with increasing p_T, but the large statistical uncertainties do not allow us to determine the trend of the R_AA. A suppression ($R_\mathrm{AA} < 0.5$) is still observed for D mesons with $p_\mathrm{T} > 25\,\mathrm{GeV}/c$. For the

JHEP03(2016)081

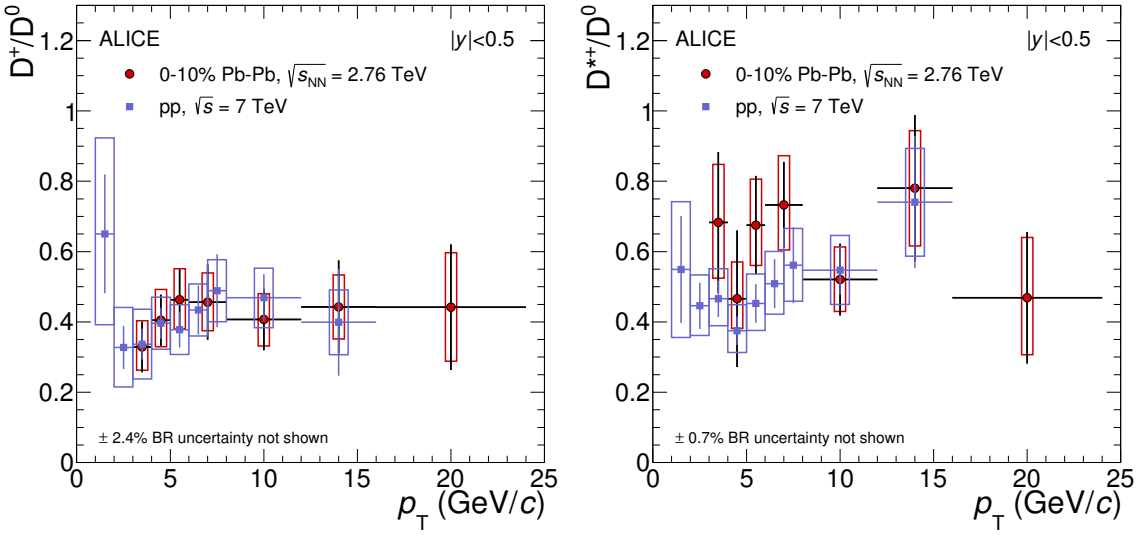

Figure 7. Ratio of prompt D-meson yields (D^+/D^0 and D^{*+}/D^0) as a function of p_T in the 10% most central Pb-Pb collisions at $\sqrt{s_{NN}} = 2.76\,\text{TeV}$ compared to the results in pp collisions at $\sqrt{s} = 7\,\text{TeV}$. Statistical (bars) and systematic (boxes) uncertainties are shown.

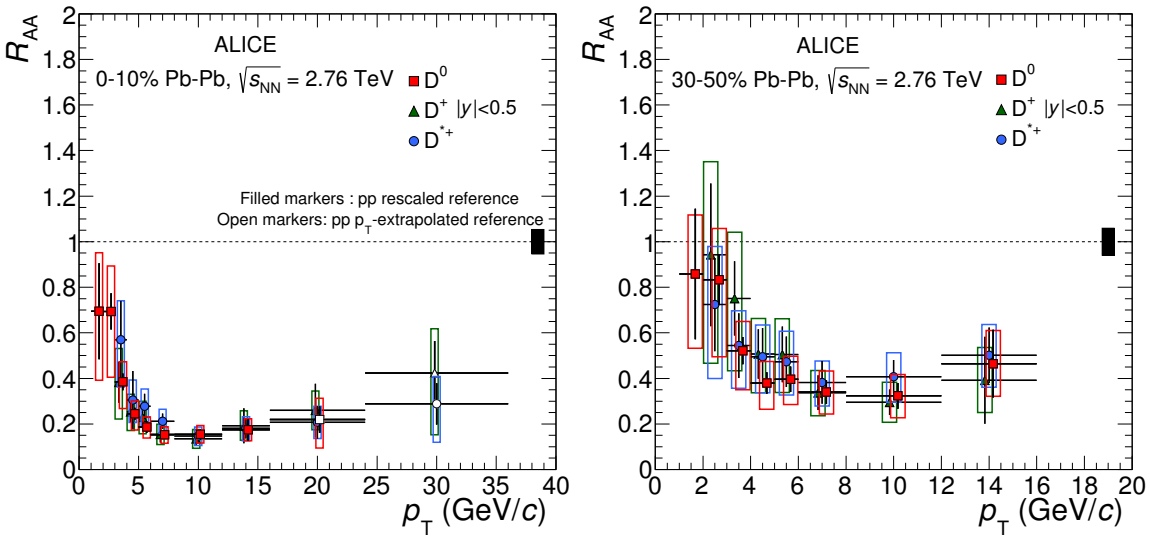

Figure 8. R_{AA} of prompt D^0, D^+, and D^{*+} mesons for the 0–10% (left) and 30–50% (right) centrality classes. Statistical (bars), systematic (empty boxes), and normalisation (shaded box) uncertainties are shown. Horizontal bars represent bin widths. D^0 symbols are placed at the centre of the bin. D^+, and D^{*+} are shifted for visibility.

30–50% centrality class, the suppression amounts to about a factor of 3 at $p_T = 10\,\text{GeV}/c$, which indicates that the suppression of the high-p_T D-meson yields is smaller than in the 0–10% centrality class. As for the central collisions, the suppression reduces at lower momenta, with R_{AA} increasing with decreasing p_T up to a value of about 0.6 in the interval $3 < p_T < 4\,\text{GeV}/c$. For lower p_T the suppression is further reduced and R_{AA} is compatible with unity.

JHEP03(2016)081

The average nuclear modification factor of D^0, D^+ and D^{*+} mesons was computed using the inverse of the squared relative statistical uncertainties as weights. The systematic uncertainties were propagated through the averaging procedure, considering the contributions from the tracking efficiency, the B-meson feed-down subtraction and the FONLL-based $\sqrt{s}$-scaling of the pp cross section from $\sqrt{s} = 7\,\text{TeV}$ to $\sqrt{s} = 2.76\,\text{TeV}$ as fully correlated uncertainties among the three D-meson species. The average D-meson R_{AA} for the two centrality classes is shown in the left panel of figure 9. A larger suppression, by about a factor of two, is observed in the 10% most central collisions compared to the 30–50% centrality class for $p_{\text{T}} > 5\,\text{GeV}/c$. The stronger suppression observed in central collisions can be understood as resulting from to the increasing medium density, size and lifetime from peripheral to central collisions. The R_{AA} values measured for the 0–10% centrality class are slightly lower, although compatible within uncertainties, than those reported in ref. [32] for the 20% most central collisions, measured with the 2010 data sample. As a consistency check, the analysis on the 2011 data sample was also performed in the 0–20% centrality class and the resulting R_{AA} value was found to be compatible with the one measured with the 2010 sample within statistical and systematic uncertainties, considering that the pp reference uncertainties are the same in the two measurements. In addition, the larger sample of central Pb-Pb collisions used in this analysis, compared to that used in the previous publication, enables the measurement of the D-meson R_{AA} in a wider p_{T} range (the intervals $1 < p_{\text{T}} < 2\,\text{GeV}/c$ and $p_{\text{T}} > 16\,\text{GeV}/c$ were not accessible with the previous sample), with a substantial reduction (by a factor of about 2–3) of the statistical uncertainties.

Figure 9 (left) also shows the average D-meson nuclear modification factor measured in minimum-bias p-Pb collisions at $\sqrt{s_{\text{NN}}} = 5.02\,\text{TeV}$ [33]. Since no significant modification of the D-meson production is observed in p-Pb collisions for $p_{\text{T}} > 2\,\text{GeV}/c$, the strong suppression of the D-meson yields for $p_{\text{T}} > 3\,\text{GeV}/c$ observed in central and semi-central Pb-Pb collisions cannot be explained in terms of cold nuclear matter effects and is predominantly due to final-state effects induced by the hot and dense medium created in the collisions.

5.2 Comparison with results at lower collision energy

In the right panel of figure 9, the average D-meson R_{AA} for the 10% most central Pb-Pb collisions is compared to the D^0 nuclear modification factor measured by the STAR Collaboration for the 10% most central Au-Au collisions at $\sqrt{s_{\text{NN}}} = 200\,\text{GeV}$ [31]. The D-meson R_{AA} measured at the two energies are compatible within uncertainties for $p_{\text{T}} > 2\,\text{GeV}/c$. It should be noted that the similar R_{AA} of D mesons with high momentum, $p_{\text{T}} > 5\,\text{GeV}/c$, i.e. in the range where the nuclear modification factor is expected to be dominated by the effect of in-medium parton energy loss, does not necessarily imply a similar charm-quark energy loss at the two collision energies. Since the nuclear modification factor is also sensitive to the slope of the p_{T} spectra in pp collisions, the combined effect of a denser medium and of the harder p_{T} spectra at the LHC could result in similar values of R_{AA} as at lower collision energies (see e.g. ref. [63]).

JHEP03(2016)081

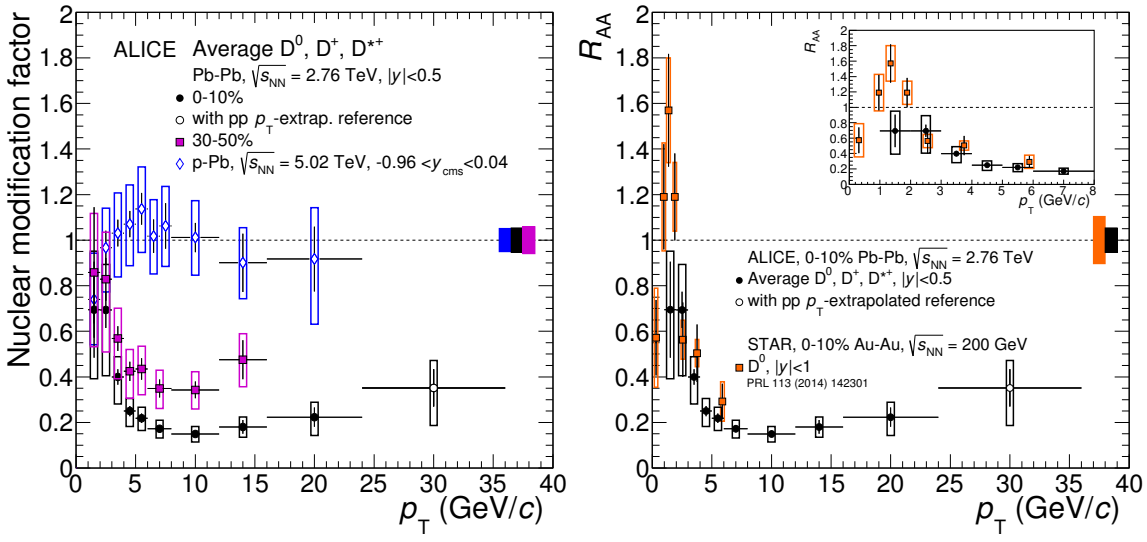

Figure 9. Left: prompt D-meson $R_{\rm AA}$ (average of $\rm D^0$, $\rm D^+$ and $\rm D^{*+}$) as a function of $p_{\rm T}$ in Pb-Pb collisions at $\sqrt{s_{\rm NN}} = 2.76\,\rm TeV$ in the 0–10% and 30–50% centrality classes. Prompt D-meson nuclear modification factor (average of $\rm D^0$, $\rm D^+$ and $\rm D^{*+}$) as a function of $p_{\rm T}$ in p-Pb collisions at $\sqrt{s_{\rm NN}} = 5.02\,\rm TeV$ [33]. Right: prompt D-meson $R_{\rm AA}$ (average of $\rm D^0$, $\rm D^+$ and $\rm D^{*+}$) as a function of $p_{\rm T}$ in the 10% most central Pb-Pb collisions at $\sqrt{s_{\rm NN}} = 2.76\,\rm TeV$ compared to $\rm D^0$ $R_{\rm AA}$ measured by the STAR Collaboration in Au-Au collisions at RHIC at $\sqrt{s_{\rm NN}} = 200\,\rm GeV$ [31]. A zoomed-in plot of the interval $0 < p_{\rm T} < 8\,\rm GeV/\mathit{c}$ is shown in the inset. Statistical (bars), systematic (empty boxes), and normalisation (shaded boxes at $R_{\rm AA} = 1$) uncertainties are shown. Horizontal bars represent bin widths. Symbols are placed at the centre of the bin.

At low momentum ($1 < p_{\rm T} < 2\,\rm GeV/\mathit{c}$), the $R_{\rm AA}$ measured by STAR shows a maximum. This effect can be described by models including parton energy loss, collective radial flow and the contribution of the recombination mechanism to charm-quark hadronisation [30]. The ALICE results at higher $\sqrt{s_{\rm NN}}$ do not show a maximum. However, the large uncertainties and the coarser binning at low $p_{\rm T}$ prevent a firm conclusion from being drawn. A different pattern could be explained by the different role of initial-state effects or of radial flow at the two collision energies. In the initial state, the modification of the parton distribution functions in a nuclear environment is predicted to lead to a stronger suppression of the heavy-quark production yields at low $p_{\rm T}$ with increasing $\sqrt{s_{\rm NN}}$ [64], because of the smaller values of Bjorken-x probed. In addition, the momentum ($k_{\rm T}$) broadening effect, which gives rise to an enhancement of the $R_{\rm AA}$ at intermediate $p_{\rm T}$ (Cronin peak), is known to be more pronounced at lower collision energies [65, 66]. In the final state, in addition to energy loss, the collective expansion of the medium is also predicted to affect the momentum distribution of charmed hadrons in heavy-ion collisions. Indeed, the interactions with the medium constituents are expected to transfer momentum to low-$p_{\rm T}$ charm quarks, which could take part in the collective radial flow of the medium. This effect could be enhanced by hadronisation via recombination, which is predicted in some models to contribute significantly to hadron formation at low and intermediate $p_{\rm T}$ [15]. The momentum distributions of identified light-flavour hadrons at

JHEP03(2016)081

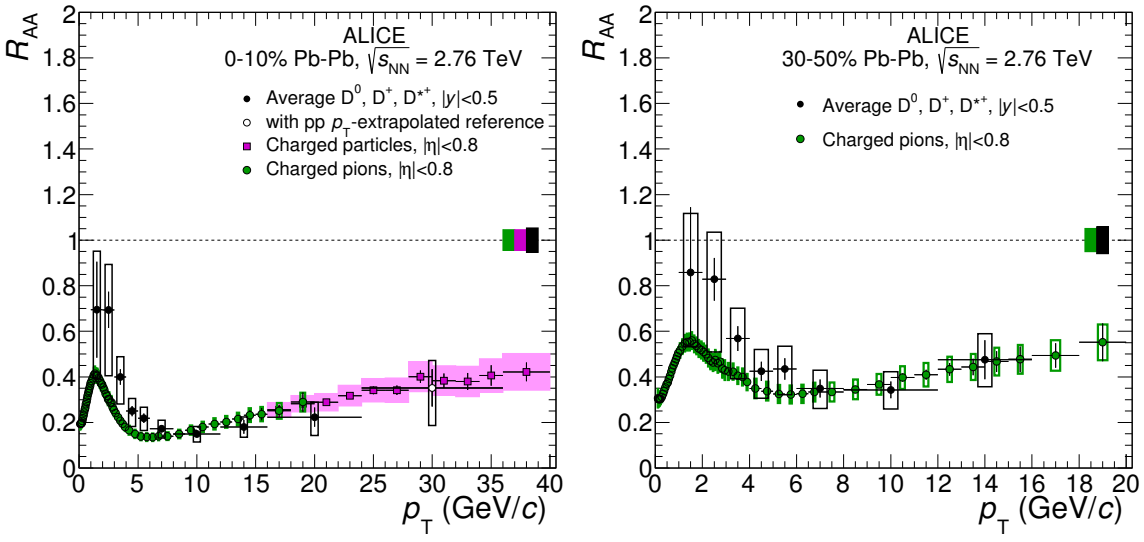

Figure 10. Prompt D-meson $R_{\rm AA}$ (average of $\rm D^0$, $\rm D^+$ and $\rm D^{*+}$) as a function of $p_{\rm T}$ compared to the nuclear modification factors of pions [72] and charged particles [73] in the 0–10% (left) and 30–50% (right) centrality classes. Statistical (bars), systematic (empty boxes), and normalisation (shaded box at $R_{\rm AA} = 1$) uncertainties are shown. Horizontal bars represent bin widths. Symbols are placed at the centre of the bin.

the LHC [67, 68] indicate that the radial flow of the medium at LHC energies is about 10% higher than at RHIC [69]. However, this stronger radial flow does not necessarily give rise to a more pronounced bump-like structure in the $R_{\rm AA}$ at low $p_{\rm T}$ with increasing collision energy, because its effect can be counterbalanced by the different shape of the momentum spectra in pp collisions at different $\sqrt{s}$ [70, 71].

5.3 Comparison with pion and charged-hadron $R_{\rm AA}$

As described in section 1, the colour-charge and quark-mass dependence of the energy loss can be tested with the comparison of D-meson and pion nuclear modification factors. In the left panel of figure 10, the D-meson $R_{\rm AA}$ (average of $\rm D^0$, $\rm D^+$ and $\rm D^{*+}$) measured for the 10% most central Pb-Pb collisions is compared with the pion $R_{\rm AA}$ in the interval $1 < p_{\rm T} < 20\,\mathrm{GeV}/c$ and with the $R_{\rm AA}$ of charged particles in $16 < p_{\rm T} < 40\,\mathrm{GeV}/c$. The charged-particle $R_{\rm AA}$ is shown in order to extend the comparison up to the higher $p_{\rm T}$ interval in which the D-meson yield was measured. The comparison of D mesons with charged hadrons at high-$p_{\rm T}$ is relevant because the $R_{\rm AA}$ of different light-flavour hadron species are consistent with one another for $p_{\rm T} > 8\,\mathrm{GeV}/c$ [72]. Moreover the contribution of pions dominates the charged-hadron yields at $p_{\rm T}$ of about $20\,\mathrm{GeV}/c$ with respect to other hadron species (about 65%) [74]. A similar comparison is performed in the right panel of figure 10 for the 30–50% centrality class.

The $R_{\rm AA}$ of D mesons and light-flavour hadrons are consistent for $p_{\rm T} > 6\,\mathrm{GeV}/c$ for both centrality classes. For $p_{\rm T} < 6\,\mathrm{GeV}/c$, the $R_{\rm AA}$ of D mesons tends to be slightly higher than that of pions. This can be also observed from the ratio of nuclear modification factors,

JHEP03(2016)081

presented in figure 13. Considering that the systematic uncertainties of D-meson yields are mainly correlated with p_{T}, we observe $R_{\mathrm{AA}}^{\mathrm{D}} > R_{\mathrm{AA}}^{\pi}$ at low p_{T} with a significance of about $1\,\sigma$ in four p_{T} intervals, in the most central events. In the 30–50% centrality class, the significance of the effect is smaller than in central collisions.

A direct interpretation of a possible difference between the D-meson and pion R_{AA} at low p_{T} is not straightforward. In the presence of a colour-charge and quark-mass dependent energy loss, the harder p_{T} distribution and the harder fragmentation function of charm quarks compared to those of light quarks and gluons could lead to similar values of D-meson and pion R_{AA}, as discussed in ref. [13]. In addition, it should be considered that the pion yield could have a substantial contribution from soft production processes up to transverse momenta of about 2–3 GeV/c due to the strong radial flow at LHC energies. This soft contribution, which is not present in the D-meson yield, does not scale with the number of binary nucleon-nucleon collisions. Finally, the effects of radial flow and hadronisation via recombination, as well as initial-state effects, could affect D-meson and pion (light-flavour particle) yields differently at a given p_{T}, thus introducing an additional complication in interpreting the magnitude of the R_{AA} in terms of different in-medium parton energy loss of charm quarks, light quarks and gluons.

5.4 Comparison with models

Figure 11 shows the comparison of the average D-meson R_{AA} for the two centrality classes 0–10% (a and b) and 30–50% (c and d) with most of the available model calculations. The model calculations are described and compared in a recent review [15]. A concise summary is given in the following paragraphs.

The interaction of heavy quarks with the medium constituents is computed considering radiative and collisional processes in the calculations indicated as *Djordjevic* [75], *WHDG* [20–22], *CUJET3.0* [76, 77], *MC@sHQ+EPOS* [80], *BAMPS* [53–55], and *Cao, Qin, Bass* [79]. Only collisional interactions are considered in the model calculations *POWLANG* [81, 82], *TAMU elastic* [70] and PHSD [83]. In *BAMPS*, two different options are considered: including only collisional energy loss but introducing a scaling factor to match RHIC high-p_{T} data (where radiative energy loss is expected to be dominant) or including both collisional and radiative energy loss. Also for the *Vitev* model [78] two different options are considered: including only radiative energy loss (*Vitev* rad) or also considering the in-medium dissociation of heavy-flavour hadrons (*Vitev* rad+dissoc).

The medium is described using an underlying hydrodynamical model in *CUJET3.0*, *Cao, Qin, Bass*, *MC@sHQ+EPOS*, *BAMPS*, *POWLANG*, *TAMU elastic* and *PHSD*, while *Djordjevic*, *WHDG* and *Vitev* use a Glauber model nuclear overlap without radial expansion.

The initial heavy-quark p_{T} distributions are based on next-to-leading order (NLO) or FONLL perturbative QCD calculations in all model calculations, except for *Cao, Qin, Bass*, which uses the PYTHIA event generator [49]. The EPS09 NLO parameterisation [64] of the nuclear parton distribution functions is included by *POWLANG*, *MC@sHQ+EPOS*, *TAMU elastic*, *PHSD* and *Cao, Qin, Bass*.

JHEP03(2016)081

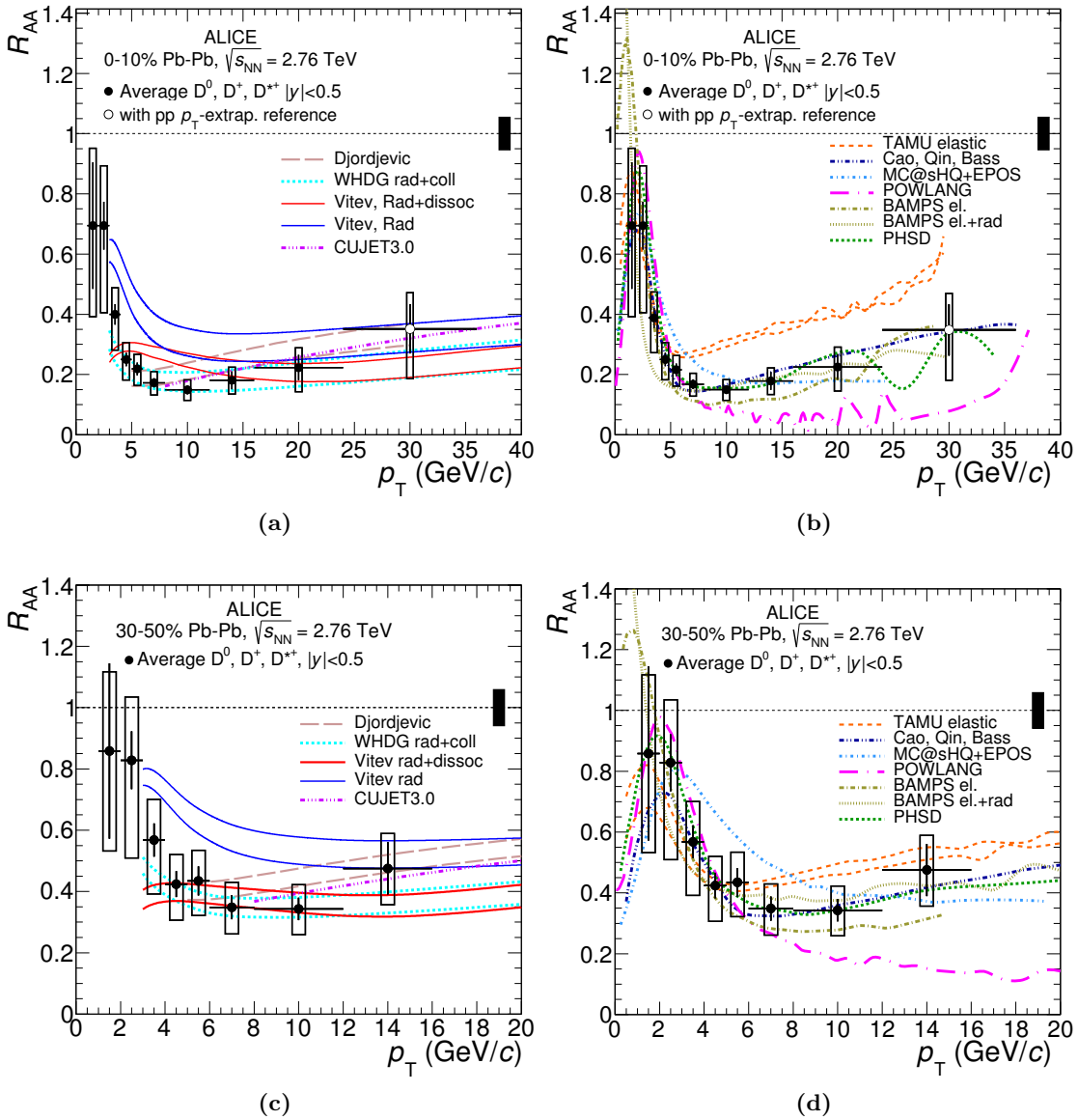

Figure 11. Average of prompt D^0, D^+ and D^{*+} R_{AA} in the centrality classes 0–10% (a and b) and 30–50% (c and d) compared with model calculations: *Djordjevic* [75], *CUJET3.0* [76, 77], *WHDG* [20–22], *Vitev* [78] (a and c), *TAMU elastic* [70], *Cao, Qin and Bass* [79], *MC@sHQ+EPOS, Coll+Rad(LPM)* [80], *POWLANG* [81, 82], *BAMPS* [53–55], *PHSD* [83] (b and d). Some of the model calculations are shown by two lines to represent their uncertainties.

All model calculations use in-vacuum fragmentation of heavy quarks for the high-momentum region. At low momentum this is supplemented by hadronisation via recombination in the *MC@sHQ+EPOS*, *POWLANG*,[2] *Cao, Qin, Bass*, *TAMU elastic* and *PHSD* models. The two last models also include scattering of D mesons in the hadronic phase

[2]Note that recombination was not included in the version of the *POWLANG* model used for the comparison with the D-meson v_2 measurement in [35].

JHEP03(2016)081

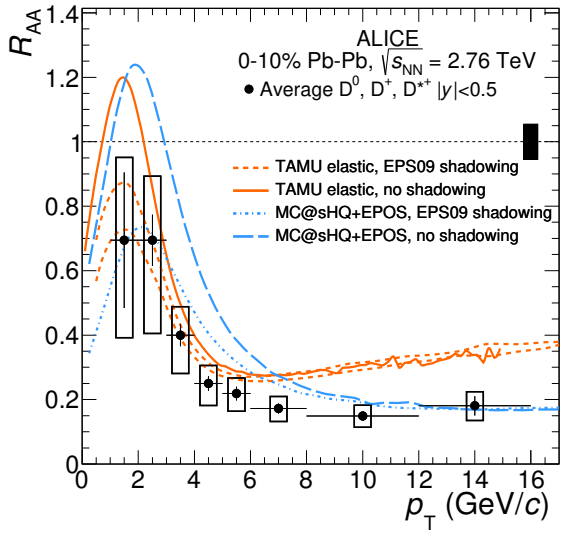

Figure 12. Average of prompt D^0, D^+ and D^{*+} R_{AA} in the centrality classes 0–10% compared with *TAMU elastic* and *MC@sHQ+EPOS* models calculations with and without including EPS09 shadowing parameterisations [64].

of the medium. Also for the *Cao, Qin, Bass* model, the hadronic-rescattering effects have been studied in a recent publication [84] and no large differences in the R_{AA} are observed, when these processes are considered.

Several model calculations provide a good description of the measured R_{AA} for both centrality classes. The *MC@sHQ+EPOS* model has recently improved the description of the R_{AA} in the p_T interval 2–8 GeV/c including the EPS09 shadowing parameterisation in addition to in-medium energy loss, the *TAMU elastic* model overestimates the R_{AA} in central collisions in the p_T interval 6–30 GeV/c and the *POWLANG* model underestimates it in the interval 5–36 (8–16) GeV/c in the 0–10% (30–50%) centrality class. Interestingly, these model calculations provide a fair description of the D-meson v_2 measured at LHC [35] and of the D-meson R_{AA} measured at RHIC [31]. On the other hand, the model calculations that do not include a hydrodynamical medium expansion and hadronisation via recombination, namely *Djordjevic*, *Vitev*, *WHDG* — and as a consequence do not describe the features observed for the v_2 at the LHC and the R_{AA} at RHIC in the momentum region up to about 3–5 GeV/c — provide a good description of the R_{AA} in the full "high p_T interval", above 5 GeV/c. The *Vitev* model shows a better agreement when including the D-meson in-medium dissociation mechanism. The BAMPS model with collisional energy loss describes the data better for the low-p_T interval, as is the case for the D-meson v_2 [35]. The inclusion of radiative energy loss improves the agreement at high p_T. The *Cao, Qin, Bass* model describes the R_{AA} in both centrality classes, but underestimates the D-meson v_2 [35]. The *PHSD* model describes the R_{AA} in both centrality classes.

Figure 12 shows the *TAMU elastic* and *MC@sHQ+EPOS* calculations of the nuclear modification factor, for the 10% most central events, with and without including the EPS09 shadowing parameterisation. For both models the inclusion of shadowing reduces the R_{AA}

JHEP03(2016)081

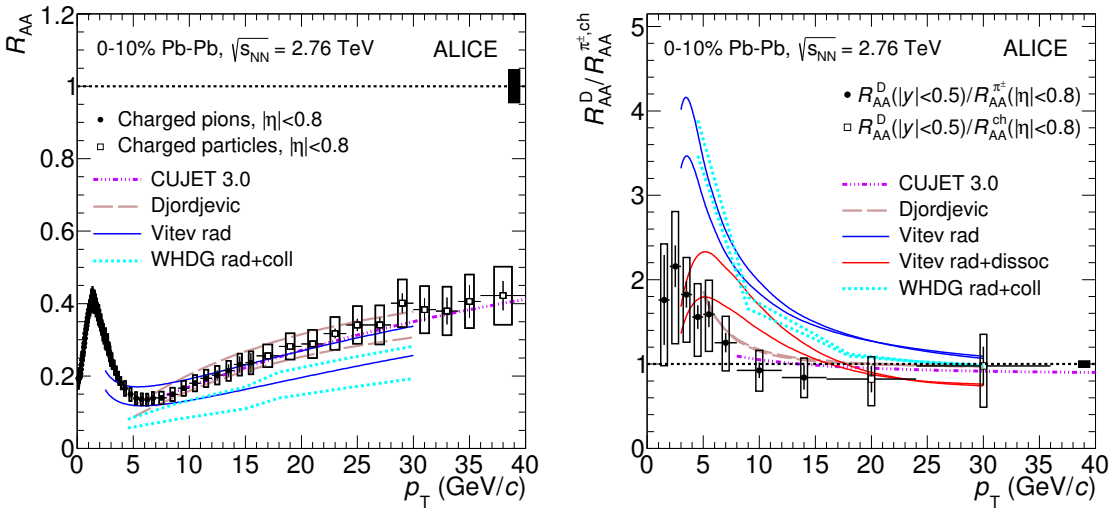

Figure 13. Left: $R_{\rm AA}$ of charged pions ($p_{\rm T} < 16\,{\rm GeV}/c$) [72] and of charged particles ($p_{\rm T} > 16\,{\rm GeV}/c$) [73] compared with model calculations that compute also the D-meson $R_{\rm AA}$. Right: ratio of the $R_{\rm AA}$ of prompt D mesons (average of $\rm D^0$, $\rm D^+$ and $\rm D^{*+}$ as shown in figure 11) and the $R_{\rm AA}$ of charged pions (for $p_{\rm T} < 20\,{\rm GeV}/c$) or charged particles (for $p_{\rm T} > 20\,{\rm GeV}/c$), compared with the same model calculations shown in the left panel.

by up to about 30–40% in the interval $p_{\rm T} < 5\,{\rm GeV}/c$, resulting in a better description of the data.

Four of the model calculations also provide the nuclear modification factor of pions and charged particles (*Djordjevic*, *CUJET3.0*, *WHDG* and *Vitev*). All these calculations include radiative and collisional energy loss.[3] The left panel of figure 13 shows the comparison with the measured charged-pion $R^{\pi}_{\rm AA}$ ($p_{\rm T} < 16\,{\rm GeV}/c$) [72] and charged-particle $R^{ch}_{\rm AA}$ ($p_{\rm T} > 16\,{\rm GeV}/c$) [73]. The model calculations provide a reasonable description of the measurements, with *WHDG* generally showing smaller $R_{\rm AA}$ values than seen in data, although consistent within experimental and theoretical uncertainties.

The right panel of figure 13 shows the $R^{\rm D}_{\rm AA}/R^{\pi}_{\rm AA}$ ($p_{\rm T} < 16\,{\rm GeV}/c$) and $R^{\rm D}_{\rm AA}/R^{ch}_{\rm AA}$ ($p_{\rm T} > 16\,{\rm GeV}/c$) ratios for data and for these four model calculations. In the case of data, the uncertainties of D-meson and charged-pion (or charged-particle) measurements were propagated as uncorrelated uncertainties, except for the uncertainty on $\langle T_{\rm AA}\rangle$, which cancels in the ratio.[4] In the case of model calculations, the theoretical uncertainty, when provided, was propagated assuming full correlation between D mesons and pions (charged particles), since it accounts for a variation of the medium density (or temperature). Only the *Djordjevic* and *CUJET3.0* models, which use radiative and collisional energy loss, can describe the two $R_{\rm AA}$ results and their ratio over the full $p_{\rm T}$ interval in which they provide

[3] The in-medium formation and dissociation process, included by *Vitev* for D mesons, is not relevant for pions, which have a much larger formation time.

[4] The uncertainty on the normalisation (integrated luminosity) of the pp reference cross sections for D mesons and pions (charged particles) does not cancel in the ratio, because the two cross sections were measured in two data samples at different centre-of-mass energies.

JHEP03(2016)081

the calculations ($p_{\rm T} > 5$ and $8\,{\rm GeV}/c$, respectively). The *Vitev* model can describe the data at the lowest $p_{\rm T}$ (2–$6\,{\rm GeV}/c$) only if the dissociation mechanism is included, suggesting that the effect is relevant in this model. However, the model overestimates the data in the interval 6–$12\,{\rm GeV}/c$.

6 Conclusions

We have presented the measurements of the production of prompt $\rm D^0$, $\rm D^+$ and $\rm D^{*+}$ mesons at central rapidity in Pb-Pb collisions at a centre-of-mass energy per nucleon pair $\sqrt{s_{\rm NN}} = 2.76\,{\rm TeV}$, as well as their nuclear modification factor $R_{\rm AA}$. The measurements cover the interval $1 < p_{\rm T} < 36\,{\rm GeV}/c$ for the 0–10% centrality class and $1 < p_{\rm T} < 16\,{\rm GeV}/c$ for the 30–50% centrality class.

The nuclear modification factor shows a maximum reduction of the yields with respect to binary scaling by a factor 5–6, for transverse momenta of about $10\,{\rm GeV}/c$ for the 10% most central Pb-Pb collisions. A suppression of a factor about 2–3 persists in the highest $p_{\rm T}$ interval covered by the measurements (24–$36\,{\rm GeV}/c$). At low $p_{\rm T}$ (1–$3\,{\rm GeV}/c$), the $R_{\rm AA}$ has large uncertainties, that span the range from 0.35 (factor of three suppression) to 1 (no suppression). In all $p_{\rm T}$ intervals above $5\,{\rm GeV}/c$, the $R_{\rm AA}$ for the 30–50% centrality class is about twice that for the 0–10% centrality class. The suppression observed for $p_{\rm T} > 3\,{\rm GeV}/c$ is interpreted to be due to interactions of the charm quarks within the high-energy density medium formed in the final-state of Pb-Pb collisions. This is demonstrated by the nuclear modification factor measurements in p-Pb collisions at $\sqrt{s_{\rm NN}} = 5.02\,{\rm TeV}$, which indicate that D-meson production is consistent with binary collision scaling [33].

The D-meson $R_{\rm AA}$ was compared with that of charged pions in the interval $1 < p_{\rm T} < 16\,{\rm GeV}/c$, also in terms of the ratio $R^{\rm D}_{\rm AA}/R^{\pi}_{\rm AA}$, and with that of charged particles up to $p_{\rm T} = 36\,{\rm GeV}/c$ ($R^{\rm D}_{\rm AA}/R^{ch}_{\rm AA}$). In the interval $1 < p_{\rm T} < 6\,{\rm GeV}/c$, the $R_{\rm AA}$ values of D mesons are higher than those of pions, although consistent within uncertainties. For the 10% most central collisions, the ratio $R^{\rm D}_{\rm AA}/R^{\pi,\,ch}_{\rm AA}$ is larger than unity by about $1\,\sigma$ of the total uncertainties, which are to some extent correlated among $p_{\rm T}$ intervals. For $p_{\rm T} > 8\,{\rm GeV}/c$, the $R_{\rm AA}$ values are compatible with those of pions and charged particles up to $p_{\rm T} = 36\,{\rm GeV}/c$.

Several models provide a good description of the $R_{\rm AA}$ for both centrality classes. Interestingly, the models that show larger deviation from the data, especially in the high-$p_{\rm T}$ region, are among those that provide a good description of the D-meson v_2 measured at the LHC and of the D-meson $R_{\rm AA}$ measured at RHIC, in the low-$p_{\rm T}$ region. On the other hand, the models that do not include a hydrodynamical medium expansion and recombination, and as a consequence do not describe v_2 in the momentum region up to about 3–$5\,{\rm GeV}/c$, provide a good description of the $R_{\rm AA}$ at the LHC in the full high-$p_{\rm T}$ interval, above $5\,{\rm GeV}/c$.

Only two out of the four models that compute $R^{\rm D}_{\rm AA}/R^{\pi,\,ch}_{\rm AA}$ can describe this measurement over the full $p_{\rm T}$ interval for which they provide the calculations. In these models, the nuclear modification factors of D mesons and pions turn out to be very similar as a consequence of a compensation among the larger energy loss of gluons with respect to that

JHEP03(2016)081

of charm quarks (mainly due to the larger colour coupling factor), the different amount of gluon and light quark yields on the pion $R_{\rm AA}$ and the harder $p_{\rm T}$ distribution and fragmentation of charm quarks with respect to those of gluons and of light quarks.

Acknowledgments

The ALICE Collaboration would like to thank all its engineers and technicians for their invaluable contributions to the construction of the experiment and the CERN accelerator teams for the outstanding performance of the LHC complex. The ALICE Collaboration gratefully acknowledges the resources and support provided by all Grid centres and the Worldwide LHC Computing Grid (WLCG) collaboration. The ALICE Collaboration acknowledges the following funding agencies for their support in building and running the ALICE detector: State Committee of Science, World Federation of Scientists (WFS) and Swiss Fonds Kidagan, Armenia; Conselho Nacional de Desenvolvimento Científico e Tecnológico (CNPq), Financiadora de Estudos e Projetos (FINEP), Fundação de Amparo à Pesquisa do Estado de São Paulo (FAPESP); National Natural Science Foundation of China (NSFC), the Chinese Ministry of Education (CMOE) and the Ministry of Science and Technology of China (MSTC); Ministry of Education and Youth of the Czech Republic; Danish Natural Science Research Council, the Carlsberg Foundation and the Danish National Research Foundation; The European Research Council under the European Community's Seventh Framework Programme; Helsinki Institute of Physics and the Academy of Finland; French CNRS-IN2P3, the 'Region Pays de Loire', 'Region Alsace', 'Region Auvergne' and CEA, France; German Bundesministerium fur Bildung, Wissenschaft, Forschung und Technologie (BMBF) and the Helmholtz Association; General Secretariat for Research and Technology, Ministry of Development, Greece; Hungarian Orszagos Tudomanyos Kutatasi Alappgrammok (OTKA) and National Office for Research and Technology (NKTH); Department of Atomic Energy and Department of Science and Technology of the Government of India; Istituto Nazionale di Fisica Nucleare (INFN) and Centro Fermi — Museo Storico della Fisica e Centro Studi e Ricerche "Enrico Fermi", Italy; MEXT Grant-in-Aid for Specially Promoted Research, Japan; Joint Institute for Nuclear Research, Dubna; National Research Foundation of Korea (NRF); Consejo Nacional de Cienca y Tecnologia (CONACYT), Direccion General de Asuntos del Personal Academico(DGAPA), México, Amerique Latine Formation academique — European Commission (ALFA-EC) and the EPLANET Program (European Particle Physics Latin American Network); Stichting voor Fundamenteel Onderzoek der Materie (FOM) and the Nederlandse Organisatie voor Wetenschappelijk Onderzoek (NWO), Netherlands; Research Council of Norway (NFR); National Science Centre, Poland; Ministry of National Education/Institute for Atomic Physics and National Council of Scientific Research in Higher Education (CNCSI-UEFISCDI), Romania; Ministry of Education and Science of Russian Federation, Russian Academy of Sciences, Russian Federal Agency of Atomic Energy, Russian Federal Agency for Science and Innovations and The Russian Foundation for Basic Research; Ministry of Education of Slovakia; Department of Science and Technology, South Africa; Centro de Investigaciones Energeticas, Medioambientales y Tecnologicas (CIEMAT), E-Infrastructure shared

JHEP03(2016)081

between Europe and Latin America (EELA), Ministerio de Economía y Competitividad (MINECO) of Spain, Xunta de Galicia (Consellería de Educación), Centro de Aplicaciones Tecnológicas y Desarrollo Nuclear (CEADEN), Cubaenergía, Cuba, and IAEA (International Atomic Energy Agency); Swedish Research Council (VR) and Knut & Alice Wallenberg Foundation (KAW); Ukraine Ministry of Education and Science; United Kingdom Science and Technology Facilities Council (STFC); The United States Department of Energy, the United States National Science Foundation, the State of Texas, and the State of Ohio; Ministry of Science, Education and Sports of Croatia and Unity through Knowledge Fund, Croatia; Council of Scientific and Industrial Research (CSIR), New Delhi, India; Pontificia Universidad Católica del Perú.

References

[1] F. Karsch, *Lattice simulations of the thermodynamics of strongly interacting elementary particles and the exploration of new phases of matter in relativistic heavy ion collisions*, *J. Phys. Conf. Ser.* **46** (2006) 122 [hep-lat/0608003] [INSPIRE].

[2] WUPPERTAL-BUDAPEST collaboration, S. Borsányi, Z. Fodor, C. Hölbling, S.D. Katz, S. Krieg, C. Ratti et al., *Is there still any T_c mystery in lattice QCD? Results with physical masses in the continuum limit III*, *JHEP* **09** (2010) 073 [arXiv:1005.3508] [INSPIRE].

[3] S. Borsányi, Z. Fodor, C. Hölbling, S.D. Katz, S. Krieg and K.K. Szabo, *Full result for the QCD equation of state with $2+1$ flavors*, *Phys. Lett.* **B 730** (2014) 99 [arXiv:1309.5258] [INSPIRE].

[4] A. Bazavov et al., *The chiral and deconfinement aspects of the QCD transition*, *Phys. Rev.* **D 85** (2012) 054503 [arXiv:1111.1710] [INSPIRE].

[5] F.-M. Liu and S.-X. Liu, *quark-gluon plasma formation time and direct photons from heavy ion collisions*, *Phys. Rev.* **C 89** (2014) 034906 [arXiv:1212.6587] [INSPIRE].

[6] M. Gyulassy and M. Plumer, *Jet Quenching in Dense Matter*, *Phys. Lett.* **B 243** (1990) 432 [INSPIRE].

[7] R. Baier, Y.L. Dokshitzer, A.H. Mueller, S. Peigne and D. Schiff, *Radiative energy loss and p_T broadening of high-energy partons in nuclei*, *Nucl. Phys.* **B 484** (1997) 265 [hep-ph/9608322] [INSPIRE].

[8] M.H. Thoma and M. Gyulassy, *Quark Damping and Energy Loss in the High Temperature QCD*, *Nucl. Phys.* **B 351** (1991) 491 [INSPIRE].

[9] E. Braaten and M.H. Thoma, *Energy loss of a heavy fermion in a hot plasma*, *Phys. Rev.* **D 44** (1991) 1298 [INSPIRE].

[10] E. Braaten and M.H. Thoma, *Energy loss of a heavy quark in the quark-gluon plasma*, *Phys. Rev.* **D 44** (1991) 2625 [INSPIRE].

[11] R.J. Glauber and G. Matthiae, *High-energy scattering of protons by nuclei*, *Nucl. Phys.* **B 21** (1970) 135 [INSPIRE].

JHEP03(2016)081

[12] M.L. Miller, K. Reygers, S.J. Sanders and P. Steinberg, *Glauber modeling in high energy nuclear collisions*, *Ann. Rev. Nucl. Part. Sci.* **57** (2007) 205 [nucl-ex/0701025] [INSPIRE].

[13] M. Djordjevic, *Heavy flavor puzzle at LHC: a serendipitous interplay of jet suppression and fragmentation*, *Phys. Rev. Lett.* **112** (2014) 042302 [arXiv:1307.4702] [INSPIRE].

[14] N. Armesto, A. Dainese, C.A. Salgado and U.A. Wiedemann, *Testing the color charge and mass dependence of parton energy loss with heavy-to-light ratios at RHIC and CERN LHC*, *Phys. Rev.* **D 71** (2005) 054027 [hep-ph/0501225] [INSPIRE].

[15] A. Andronic et al., *Heavy-flavour and quarkonium production in the LHC era: from proton-proton to heavy-ion collisions*, arXiv:1506.03981 [INSPIRE].

[16] Y.L. Dokshitzer and D.E. Kharzeev, *Heavy quark colorimetry of QCD matter*, *Phys. Lett.* **B 519** (2001) 199 [hep-ph/0106202] [INSPIRE].

[17] N. Armesto, C.A. Salgado and U.A. Wiedemann, *Medium induced gluon radiation off massive quarks fills the dead cone*, *Phys. Rev.* **D 69** (2004) 114003 [hep-ph/0312106] [INSPIRE].

[18] M. Djordjevic and M. Gyulassy, *Heavy quark radiative energy loss in QCD matter*, *Nucl. Phys.* **A 733** (2004) 265 [nucl-th/0310076] [INSPIRE].

[19] B.-W. Zhang, E. Wang and X.-N. Wang, *Heavy quark energy loss in nuclear medium*, *Phys. Rev. Lett.* **93** (2004) 072301 [nucl-th/0309040] [INSPIRE].

[20] S. Wicks, W.A. Horowitz, M. Djordjevic and M. Gyulassy, *Elastic, inelastic and path length fluctuations in jet tomography*, *Nucl. Phys.* **A 784** (2007) 426 [nucl-th/0512076] [INSPIRE].

[21] W.A. Horowitz and M. Gyulassy, *The Surprising Transparency of the sQGP at LHC*, *Nucl. Phys.* **A 872** (2011) 265 [arXiv:1104.4958] [INSPIRE].

[22] W.A. Horowitz, *Testing pQCD and AdS/CFT Energy Loss at RHIC and LHC*, *AIP Conf. Proc.* **1441** (2012) 889 [arXiv:1108.5876] [INSPIRE].

[23] H. van Hees, V. Greco and R. Rapp, *Heavy-quark probes of the quark-gluon plasma at RHIC*, *Phys. Rev.* **C 73** (2006) 034913 [nucl-th/0508055] [INSPIRE].

[24] S. Batsouli, S. Kelly, M. Gyulassy and J.L. Nagle, *Does the charm flow at RHIC?*, *Phys. Lett.* **B 557** (2003) 26 [nucl-th/0212068] [INSPIRE].

[25] V. Greco, C.M. Ko and R. Rapp, *Quark coalescence for charmed mesons in ultrarelativistic heavy ion collisions*, *Phys. Lett.* **B 595** (2004) 202 [nucl-th/0312100] [INSPIRE].

[26] A. Andronic, P. Braun-Munzinger, K. Redlich and J. Stachel, *Statistical hadronization of charm in heavy ion collisions at SPS, RHIC and LHC*, *Phys. Lett.* **B 571** (2003) 36 [nucl-th/0303036] [INSPIRE].

[27] PHENIX collaboration, S.S. Adler et al., *Nuclear modification of electron spectra and implications for heavy quark energy loss in $Au + Au$ collisions at $\sqrt{s_{NN}} = 200$ GeV*, *Phys. Rev. Lett.* **96** (2006) 032301 [nucl-ex/0510047] [INSPIRE].

[28] PHENIX collaboration, A. Adare et al., *Heavy Quark Production in $p + p$ and Energy Loss and Flow of Heavy Quarks in $Au + Au$ Collisions at $\sqrt{s_{NN}} = 200$ GeV*, *Phys. Rev.* **C 84** (2011) 044905 [arXiv:1005.1627] [INSPIRE].

[29] PHENIX collaboration, A. Adare et al., *Nuclear-Modification Factor for Open-Heavy-Flavor Production at Forward Rapidity in $Cu + Cu$ Collisions at $\sqrt{s_{NN}} = 200$ GeV*, *Phys. Rev.* **C 86** (2012) 024909 [arXiv:1204.0754] [INSPIRE].

JHEP03(2016)081

[30] STAR collaboration, B.I. Abelev et al., *Transverse momentum and centrality dependence of high-$p_{\rm T}$ non-photonic electron suppression in Au + Au collisions at $\sqrt{s_{\rm NN}} = 200$ GeV*, *Phys. Rev. Lett.* **98** (2007) 192301 [*Erratum ibid.* **106** (2011) 159902] [nucl-ex/0607012] [INSPIRE].

[31] STAR collaboration, L. Adamczyk et al., *Observation of D^0 Meson Nuclear Modifications in Au + Au Collisions at $\sqrt{s_{\rm NN}} = 200$ GeV*, *Phys. Rev. Lett.* **113** (2014) 142301 [arXiv:1404.6185] [INSPIRE].

[32] ALICE collaboration, *Suppression of high transverse momentum D mesons in central Pb-Pb collisions at $\sqrt{s_{\rm NN}} = 2.76$ TeV*, *JHEP* **09** (2012) 112 [arXiv:1203.2160] [INSPIRE].

[33] ALICE collaboration, *Measurement of prompt D-meson production in p-Pb collisions at $\sqrt{s_{\rm NN}} = 5.02$ TeV*, *Phys. Rev. Lett.* **113** (2014) 232301 [arXiv:1405.3452] [INSPIRE].

[34] ALICE collaboration, *D meson elliptic flow in non-central Pb-Pb collisions at $\sqrt{s_{\rm NN}} = 2.76$ TeV*, *Phys. Rev. Lett.* **111** (2013) 102301 [arXiv:1305.2707] [INSPIRE].

[35] ALICE collaboration, *Azimuthal anisotropy of D meson production in Pb-Pb collisions at $\sqrt{s_{\rm NN}} = 2.76$ TeV*, *Phys. Rev.* **C 90** (2014) 034904 [arXiv:1405.2001] [INSPIRE].

[36] ALICE collaboration, *The ALICE experiment at the CERN LHC*, 2008 *JINST* **3** S08002 [INSPIRE].

[37] ALICE collaboration, *Performance of the ALICE Experiment at the CERN LHC*, *Int. J. Mod. Phys.* **A 29** (2014) 1430044 [arXiv:1402.4476] [INSPIRE].

[38] ALICE collaboration, *Performance of the ALICE VZERO system*, 2013 *JINST* **8** P10016 [arXiv:1306.3130] [INSPIRE].

[39] ALICE collaboration, *Centrality determination of Pb-Pb collisions at $\sqrt{s_{\rm NN}} = 2.76$ TeV with ALICE*, *Phys. Rev.* **C 88** (2013) 044909 [arXiv:1301.4361] [INSPIRE].

[40] R. Fruhwirth, *Application of Kalman filtering to track and vertex fitting*, *Nucl. Instrum. Meth.* **A 262** (1987) 444 [INSPIRE].

[41] ALICE collaboration, *The ALICE TPC, a large 3-dimensional tracking device with fast readout for ultra-high multiplicity events*, *Nucl. Instrum. Meth.* **A 622** (2010) 316 [arXiv:1001.1950] [INSPIRE].

[42] ALICE collaboration, *Alignment of the ALICE Inner Tracking System with cosmic-ray tracks*, 2010 *JINST* **5** P03003 [arXiv:1001.0502] [INSPIRE].

[43] A. Akindinov et al., *Performance of the ALICE Time-Of-Flight detector at the LHC*, *Eur. Phys. J. Plus* **128** (2013) 44 [INSPIRE].

[44] Particle Data Group collaboration, K.A. Olive et al., *Review of Particle Physics*, *Chin. Phys.* **C 38** (2014) 090001 [INSPIRE].

[45] ALICE collaboration, *Measurement of charm production at central rapidity in proton-proton collisions at $\sqrt{s} = 7$ TeV*, *JHEP* **01** (2012) 128 [arXiv:1111.1553] [INSPIRE].

[46] P.Z. Skands, *The Perugia Tunes*, in *Proceedings of the First International Workshop on Multiple Partonic Interactions at the LHC. MPI'08. October 27–31, 2008. Perugia, Italy*, P. Bartalini and L. Fanò eds., Verlag Deutsches Elektronen-Synchrotron, Hamburg Germany (2009), pp. 284–297, FERMILAB-CONF-09-113 [arXiv:0905.3418] [INSPIRE].

[47] R. Brun, F. Carminati and S. Giani, *GEANT Detector Description and Simulation Tool*, CERN-W5013, (1994) [INSPIRE].

JHEP03(2016)081

[48] X.-N. Wang and M. Gyulassy, *HIJING: A Monte Carlo model for multiple jet production in pp, pA and AA collisions*, *Phys. Rev.* **D 44** (1991) 3501 [INSPIRE].

[49] T. Sjöstrand, S. Mrenna and P.Z. Skands, *PYTHIA 6.4 Physics and Manual*, *JHEP* **05** (2006) 026 [hep-ph/0603175] [INSPIRE].

[50] P.Z. Skands, *Tuning Monte Carlo Generators: The Perugia Tunes*, *Phys. Rev.* **D 82** (2010) 074018 [arXiv:1005.3457] [INSPIRE].

[51] M. Cacciari, M. Greco and P. Nason, *The $p_{\rm T}$ spectrum in heavy flavor hadroproduction*, *JHEP* **05** (1998) 007 [hep-ph/9803400] [INSPIRE].

[52] M. Cacciari, S. Frixione and P. Nason, *The $p_{\rm T}$ spectrum in heavy flavor photoproduction*, *JHEP* **03** (2001) 006 [hep-ph/0102134] [INSPIRE].

[53] J. Uphoff, O. Fochler, Z. Xu and C. Greiner, *Elliptic Flow and Energy Loss of Heavy Quarks in Ultra-Relativistic heavy Ion Collisions*, *Phys. Rev.* **C 84** (2011) 024908 [arXiv:1104.2295] [INSPIRE].

[54] O. Fochler, J. Uphoff, Z. Xu and C. Greiner, *Jet quenching and elliptic flow at RHIC and LHC within a pQCD-based partonic transport model*, *J. Phys.* **G 38** (2011) 124152 [arXiv:1107.0130] [INSPIRE].

[55] J. Uphoff, O. Fochler, Z. Xu and C. Greiner, *Open Heavy Flavor in $Pb+Pb$ Collisions at $\sqrt{s}=2.76$ TeV within a Transport Model*, *Phys. Lett.* **B 717** (2012) 430 [arXiv:1205.4945] [INSPIRE].

[56] M. Cacciari, S. Frixione, N. Houdeau, M.L. Mangano, P. Nason and G. Ridolfi, *Theoretical predictions for charm and bottom production at the LHC*, *JHEP* **10** (2012) 137 [arXiv:1205.6344] [INSPIRE].

[57] D.J. Lange, *The EvtGen particle decay simulation package*, *Nucl. Instrum. Meth.* **A 462** (2001) 152 [INSPIRE].

[58] ALICE collaboration, *Centrality dependence of high-p_T D meson suppression in Pb-Pb collisions at $\sqrt{s_{\rm NN}}=2.76$ TeV*, *JHEP* **11** (2015) 205 [arXiv:1506.06604] [INSPIRE].

[59] CMS collaboration, *J/ψ results from CMS in PbPb collisions, with 150mub-1 data*, CMS-PAS-HIN-12-014, (2012) [INSPIRE].

[60] ALICE collaboration, *Measurement of charm production at central rapidity in proton-proton collisions at $\sqrt{s}=2.76$ TeV*, *JHEP* **07** (2012) 191 [arXiv:1205.4007] [INSPIRE].

[61] Z. Conesa del Valle et al., *Quarkonium production in high energy proton-proton and proton-nucleus collisions*, *Nucl. Phys. Proc. Suppl.* **214** (2011) 3 [arXiv:1105.4545] [INSPIRE].

[62] ALICE collaboration, *D_s^+ meson production at central rapidity in proton–proton collisions at $\sqrt{s}=7$ TeV*, *Phys. Lett.* **B 718** (2012) 279 [arXiv:1208.1948] [INSPIRE].

[63] R. Baier, *Jet quenching*, *Nucl. Phys.* **A 715** (2003) 209 [hep-ph/0209038] [INSPIRE].

[64] K.J. Eskola, H. Paukkunen and C.A. Salgado, *EPS09: A New Generation of NLO and LO Nuclear Parton Distribution Functions*, *JHEP* **04** (2009) 065 [arXiv:0902.4154] [INSPIRE].

[65] X.-N. Wang, *Systematic study of high $p_{\rm T}$ hadron spectra in pp, pA and AA collisions from SPS to RHIC energies*, *Phys. Rev.* **C 61** (2000) 064910 [nucl-th/9812021] [INSPIRE].

JHEP03(2016)081

[66] HARD PROBE collaboration, R. Vogt, *The A dependence of open charm and bottom production*, *Int. J. Mod. Phys.* **E 12** (2003) 211 [hep-ph/0111271] [INSPIRE].

[67] ALICE collaboration, *Pion, Kaon and Proton Production in Central Pb-Pb Collisions at* $\sqrt{s_{\rm NN}} = 2.76$ *TeV*, *Phys. Rev. Lett.* **109** (2012) 252301 [arXiv:1208.1974] [INSPIRE].

[68] ALICE collaboration, *Centrality dependence of* π*, K, p production in Pb-Pb collisions at* $\sqrt{s_{\rm NN}} = 2.76$ *TeV*, *Phys. Rev.* **C 88** (2013) 044910 [arXiv:1303.0737] [INSPIRE].

[69] STAR collaboration, B.I. Abelev et al., *Systematic Measurements of Identified Particle Spectra in pp,* $d+Au$ *and* $Au+Au$ *Collisions from STAR*, *Phys. Rev.* **C 79** (2009) 034909 [arXiv:0808.2041] [INSPIRE].

[70] M. He, R.J. Fries and R. Rapp, *Heavy Flavor at the Large Hadron Collider in a Strong Coupling Approach*, *Phys. Lett.* **B 735** (2014) 445 [arXiv:1401.3817] [INSPIRE].

[71] M. He, R.J. Fries and R. Rapp, *Heavy-Quark Diffusion and Hadronization in quark-gluon Plasma*, *Phys. Rev.* **C 86** (2012) 014903 [arXiv:1106.6006] [INSPIRE].

[72] ALICE collaboration, *Production of charged pions, kaons and protons at large transverse momenta in pp and Pb-Pb collisions at* $\sqrt{s_{\rm NN}} = 2.76$ *TeV*, *Phys. Lett.* **B 736** (2014) 196 [arXiv:1401.1250] [INSPIRE].

[73] ALICE collaboration, *Centrality Dependence of Charged Particle Production at Large Transverse Momentum in Pb-Pb Collisions at* $\sqrt{s_{\rm NN}} = 2.76$ *TeV*, *Phys. Lett.* **B 720** (2013) 52 [arXiv:1208.2711] [INSPIRE].

[74] ALICE collaboration, *Centrality dependence of the nuclear modification factor of charged pions, kaons and protons in Pb-Pb collisions at* $\sqrt{s_{\rm NN}} = 2.76$ *TeV*, arXiv:1506.07287 [INSPIRE].

[75] M. Djordjevic, M. Djordjevic and B. Blagojevic, *RHIC and LHC jet suppression in non-central collisions*, *Phys. Lett.* **B 737** (2014) 298 [arXiv:1405.4250] [INSPIRE].

[76] J. Xu, J. Liao and M. Gyulassy, *Consistency of Perfect Fluidity and Jet Quenching in semi-quark-gluon Monopole Plasmas*, *Chin. Phys. Lett.* **32** (2015) 092501 [arXiv:1411.3673] [INSPIRE].

[77] J. Xu, J. Liao and M. Gyulassy, *Bridging Soft-Hard Transport Properties of quark-gluon Plasmas with CUJET3.0*, arXiv:1508.00552 [INSPIRE].

[78] R. Sharma, I. Vitev and B.-W. Zhang, *Light-cone wave function approach to open heavy flavor dynamics in QCD matter*, *Phys. Rev.* **C 80** (2009) 054902 [arXiv:0904.0032] [INSPIRE].

[79] S. Cao, G.-Y. Qin and S.A. Bass, *Heavy-quark dynamics and hadronization in ultrarelativistic heavy-ion collisions: Collisional versus radiative energy loss*, *Phys. Rev.* **C 88** (2013) 044907 [arXiv:1308.0617] [INSPIRE].

[80] M. Nahrgang, J. Aichelin, P.B. Gossiaux and K. Werner, *Influence of hadronic bound states above* T_c *on heavy-quark observables in* $Pb+Pb$ *collisions at the CERN Large Hadron Collider*, *Phys. Rev.* **C 89** (2014) 014905 [arXiv:1305.6544] [INSPIRE].

[81] W.M. Alberico et al., *Heavy-flavour spectra in high energy nucleus-nucleus collisions*, *Eur. Phys. J.* **C 71** (2011) 1666 [arXiv:1101.6008] [INSPIRE].

JHEP03(2016)081

[82] A. Beraudo, A. De Pace, M. Monteno, M. Nardi and F. Prino, *Heavy flavors in heavy-ion collisions: quenching, flow and correlations*, *Eur. Phys. J.* **C 75** (2015) 121 [arXiv:1410.6082] [INSPIRE].

[83] T. Song, H. Berrehrah, D. Cabrera, W. Cassing and E. Bratkovskaya, *Charm production in $Pb + Pb$ collisions at the Large Hadron Collider energy*, arXiv:1512.00891 [INSPIRE].

[84] S. Cao, G.-Y. Qin and S.A. Bass, *Energy loss, hadronization and hadronic interactions of heavy flavors in relativistic heavy-ion collisions*, *Phys. Rev.* **C 92** (2015) 024907 [arXiv:1505.01413] [INSPIRE].

JHEP03(2016)081

The ALICE collaboration

J. Adam[40] , D. Adamová[83] , M.M. Aggarwal[87] , G. Aglieri Rinella[36] , M. Agnello[110] , N. Agrawal[48] , Z. Ahammed[132] , S.U. Ahn[68] , S. Aiola[136] , A. Akindinov[58] , S.N. Alam[132] , D. Aleksandrov[99] , B. Alessandro[110] , D. Alexandre[101] , R. Alfaro Molina[64] , A. Alici[12,104] , A. Alkin[3] , J.R.M. Almaraz[119] , J. Alme[38] , T. Alt[43] , S. Altinpinar[18] , I. Altsybeev[131] , C. Alves Garcia Prado[120] , C. Andrei[78] , A. Andronic[96] , V. Anguelov[93] , J. Anielski[54] , T. Antičić[97] , F. Antinori[107] , P. Antonioli[104] , L. Aphecetche[113] , H. Appelshäuser[53] , S. Arcelli[28] , R. Arnaldi[110] , O.W. Arnold[37,92] , I.C. Arsene[22] , M. Arslandok[53] , B. Audurier[113] , A. Augustinus[36] , R. Averbeck[96] , M.D. Azmi[19] , A. Badalà[106] , Y.W. Baek[67,44] , S. Bagnasco[110] , R. Bailhache[53] , R. Bala[90] , A. Baldisseri[15] , R.C. Baral[61] , A.M. Barbano[27] , R. Barbera[29] , F. Barile[33] , G.G. Barnaföldi[135] , L.S. Barnby[101] , V. Barret[70] , P. Bartalini[7] , K. Barth[36] , J. Bartke[117] , E. Bartsch[53] , M. Basile[28] , N. Bastid[70] , S. Basu[132] , B. Bathen[54] , G. Batigne[113] , A. Batista Camejo[70] , B. Batyunya[66] , P.C. Batzing[22] , I.G. Bearden[80] , H. Beck[53] , C. Bedda[110] , N.K. Behera[50] , I. Belikov[55] , F. Bellini[28] , H. Bello Martinez[2] , R. Bellwied[122] , R. Belmont[134] , E. Belmont-Moreno[64] , V. Belyaev[75] , G. Bencedi[135] , S. Beole[27] , I. Berceanu[78] , A. Bercuci[78] , Y. Berdnikov[85] , D. Berenyi[135] , R.A. Bertens[57] , D. Berzano[36] , L. Betev[36] , A. Bhasin[90] , I.R. Bhat[90] , A.K. Bhati[87] , B. Bhattacharjee[45] , J. Bhom[128] , L. Bianchi[122] , N. Bianchi[72] , C. Bianchin[57,134] , J. Bielčík[40] , J. Bielčíková[83] , A. Bilandzic[80] , R. Biswas[4] , S. Biswas[79] , S. Bjelogrlic[57] , J.T. Blair[118] , D. Blau[99] , C. Blume[53] , F. Bock[93,74] , A. Bogdanov[75] , H. Bøggild[80] , L. Boldizsár[135] , M. Bombara[41] , J. Book[53] , H. Borel[15] , A. Borissov[95] , M. Borri[82,124] , F. Bossú[65] , E. Botta[27] , S. Böttger[52] , C. Bourjau[80] , P. Braun-Munzinger[96] , M. Bregant[120] , T. Breitner[52] , T.A. Broker[53] , T.A. Browning[94] , M. Broz[40] , E.J. Brucken[46] , E. Bruna[110] , G.E. Bruno[33] , D. Budnikov[98] , H. Buesching[53] , S. Bufalino[27,36] , P. Buncic[36] , O. Busch[93,128] , Z. Buthelezi[65] , J.B. Butt[16] , J.T. Buxton[20] , D. Caffarri[36] , X. Cai[7] , H. Caines[136] , L. Calero Diaz[72] , A. Caliva[57] , E. Calvo Villar[102] , P. Camerini[26] , F. Carena[36] , W. Carena[36] , F. Carnesecchi[28] , J. Castillo Castellanos[15] , A.J. Castro[125] , E.A.R. Casula[25] , C. Ceballos Sanchez[9] , J. Cepila[40] , P. Cerello[110] , J. Cerkala[115] , B. Chang[123] , S. Chapeland[36] , M. Chartier[124] , J.L. Charvet[15] , S. Chattopadhyay[132] , S. Chattopadhyay[100] , V. Chelnokov[3] , M. Cherney[86] , C. Cheshkov[130] , B. Cheynis[130] , V. Chibante Barroso[36] , D.D. Chinellato[121] , S. Cho[50] , P. Chochula[36] , K. Choi[95] , M. Chojnacki[80] , S. Choudhury[132] , P. Christakoglou[81] , C.H. Christensen[80] , P. Christiansen[34] , T. Chujo[128] , S.U. Chung[95] , C. Cicalo[105] , L. Cifarelli[12,28] , F. Cindolo[104] , J. Cleymans[89] , F. Colamaria[33] , D. Colella[33,36] , A. Collu[74,25] , M. Colocci[28] , G. Conesa Balbastre[71] , Z. Conesa del Valle[51] , M.E. Connors[ii,136] , J.G. Contreras[40] , T.M. Cormier[84] , Y. Corrales Morales[110] , I. Cortés Maldonado[2] , P. Cortese[32] , M.R. Cosentino[120] , F. Costa[36] , P. Crochet[70] , R. Cruz Albino[11] , E. Cuautle[63] , L. Cunqueiro[36] , T. Dahms[92,37] , A. Dainese[107] , A. Danu[62] , D. Das[100] , I. Das[51,100] , S. Das[4] , A. Dash[121,79] , S. Dash[48] , S. De[120] , A. De Caro[31,12] , G. de Cataldo[103] , C. de Conti[120] , J. de Cuveland[43] , A. De Falco[25] , D. De Gruttola[12,31] , N. De Marco[110] , S. De Pasquale[31] , A. Deisting[96,93] , A. Deloff[77] , E. Dénes[135,i], C. Deplano[81] , P. Dhankher[48] , D. Di Bari[33] , A. Di Mauro[36] , P. Di Nezza[72] , M.A. Diaz Corchero[10] , T. Dietel[89] , P. Dillenseger[53] , R. Divià[36] , Ø. Djuvsland[18] , A. Dobrin[57,81] , D. Domenicis Gimenez[120] , B. Dönigus[53] , O. Dordic[22] , T. Drozhzhova[53] , A.K. Dubey[132] , A. Dubla[57] , L. Ducroux[130] , P. Dupieux[70] , R.J. Ehlers[136] , D. Elia[103] , H. Engel[52] , E. Epple[136] , B. Erazmus[113] , I. Erdemir[53] , F. Erhardt[129] , B. Espagnon[51] , M. Estienne[113] , S. Esumi[128] , J. Eum[95] , D. Evans[101] , S. Evdokimov[111] , G. Eyyubova[40] , L. Fabbietti[92,37] , D. Fabris[107] , J. Faivre[71] , A. Fantoni[72] , M. Fasel[74] , L. Feldkamp[54] , A. Feliciello[110] , G. Feofilov[131] , J. Ferencei[83] , A. Fernández Téllez[2] , E.G. Ferreiro[17] , A. Ferretti[27] , A. Festanti[30] , V.J.G. Feuillard[15,70] , J. Figiel[117] , M.A.S. Figueredo[124,120] , S. Filchagin[98] , D. Finogeev[56] , F.M. Fionda[25] , E.M. Fiore[33] , M.G. Fleck[93] , M. Floris[36] ,

JHEP03(2016)081

S. Foertsch[65], P. Foka[96], S. Fokin[99], E. Fragiacomo[109], A. Francescon[30,36], U. Frankenfeld[96], U. Fuchs[36], C. Furget[71], A. Furs[56], M. Fusco Girard[31], J.J. Gaardhøje[80], M. Gagliardi[27], A.M. Gago[102], M. Gallio[27], D.R. Gangadharan[74], P. Ganoti[36,88], C. Gao[7], C. Garabatos[96], E. Garcia-Solis[13], C. Gargiulo[36], P. Gasik[37,92], E.F. Gauger[118], M. Germain[113], A. Gheata[36], M. Gheata[62,36], P. Ghosh[132], S.K. Ghosh[4], P. Gianotti[72], P. Giubellino[36,110], P. Giubilato[30], E. Gladysz-Dziadus[117], P. Glässel[93], D.M. Goméz Coral[64], A. Gomez Ramirez[52], V. Gonzalez[10], P. González-Zamora[10], S. Gorbunov[43], L. Görlich[117], S. Gotovac[116], V. Grabski[64], O.A. Grachov[136], L.K. Graczykowski[133], K.L. Graham[101], A. Grelli[57], A. Grigoras[36], C. Grigoras[36], V. Grigoriev[75], A. Grigoryan[1], S. Grigoryan[66], B. Grinyov[3], N. Grion[109], J.M. Gronefeld[96], J.F. Grosse-Oetringhaus[36], J.-Y. Grossiord[130], R. Grosso[96], F. Guber[56], R. Guernane[71], B. Guerzoni[28], K. Gulbrandsen[80], T. Gunji[127], A. Gupta[90], R. Gupta[90], R. Haake[54], Ø. Haaland[18], C. Hadjidakis[51], M. Haiduc[62], H. Hamagaki[127], G. Hamar[135], J.W. Harris[136], A. Harton[13], D. Hatzifotiadou[104], S. Hayashi[127], S.T. Heckel[53], M. Heide[54], H. Helstrup[38], A. Herghelegiu[78], G. Herrera Corral[11], B.A. Hess[35], K.F. Hetland[38], H. Hillemanns[36], B. Hippolyte[55], R. Hosokawa[128], P. Hristov[36], M. Huang[18], T.J. Humanic[20], N. Hussain[45], T. Hussain[19], D. Hutter[43], D.S. Hwang[21], R. Ilkaev[98], M. Inaba[128], M. Ippolitov[75,99], M. Irfan[19], M. Ivanov[96], V. Ivanov[85], V. Izucheev[111], P.M. Jacobs[74], M.B. Jadhav[48], S. Jadlovska[115], J. Jadlovsky[115,59], C. Jahnke[120], M.J. Jakubowska[133], H.J. Jang[68], M.A. Janik[133], P.H.S.Y. Jayarathna[122], C. Jena[30], S. Jena[122], R.T. Jimenez Bustamante[96], P.G. Jones[101], H. Jung[44], A. Jusko[101], P. Kalinak[59], A. Kalweit[36], J. Kamin[53], J.H. Kang[137], V. Kaplin[75], S. Kar[132], A. Karasu Uysal[69], O. Karavichev[56], T. Karavicheva[56], L. Karayan[96,93], E. Karpechev[56], U. Kebschull[52], R. Keidel[138], D.L.D. Keijdener[57], M. Keil[36], M. Mohisin Khan[19], P. Khan[100], S.A. Khan[132], A. Khanzadeev[85], Y. Kharlov[111], B. Kileng[38], D.W. Kim[44], D.J. Kim[123], D. Kim[137], H. Kim[137], J.S. Kim[44], M. Kim[44], M. Kim[137], S. Kim[21], T. Kim[137], S. Kirsch[43], I. Kisel[43], S. Kiselev[58], A. Kisiel[133], G. Kiss[135], J.L. Klay[6], C. Klein[53], J. Klein[36,93], C. Klein-Bösing[54], S. Klewin[93], A. Kluge[36], M.L. Knichel[93], A.G. Knospe[118], T. Kobayashi[128], C. Kobdaj[114], M. Kofarago[36], T. Kollegger[96,43], A. Kolojvari[131], V. Kondratiev[131], N. Kondratyeva[75], E. Kondratyuk[111], A. Konevskikh[56], M. Kopcik[115], M. Kour[90], C. Kouzinopoulos[36], O. Kovalenko[77], V. Kovalenko[131], M. Kowalski[117], G. Koyithatta Meethaleveedu[48], I. Králik[59], A. Kravčáková[41], M. Kretz[43], M. Krivda[59,101], F. Krizek[83], E. Kryshen[36], M. Krzewicki[43], A.M. Kubera[20], V. Kučera[83], C. Kuhn[55], P.G. Kuijer[81], A. Kumar[90], J. Kumar[48], L. Kumar[87], S. Kumar[48], P. Kurashvili[77], A. Kurepin[56], A.B. Kurepin[56], A. Kuryakin[98], M.J. Kweon[50], Y. Kwon[137], S.L. La Pointe[110], P. La Rocca[29], P. Ladron de Guevara[11], C. Lagana Fernandes[120], I. Lakomov[36], R. Langoy[42], C. Lara[52], A. Lardeux[15], A. Lattuca[27], E. Laudi[36], R. Lea[26], L. Leardini[93], G.R. Lee[101], S. Lee[137], F. Lehas[81], R.C. Lemmon[82], V. Lenti[103], E. Leogrande[57], I. León Monzón[119], H. León Vargas[64], M. Leoncino[27], P. Lévai[135], S. Li[70,7], X. Li[14], J. Lien[42], R. Lietava[101], S. Lindal[22], V. Lindenstruth[43], C. Lippmann[96], M.A. Lisa[20], H.M. Ljunggren[34], D.F. Lodato[57], P.I. Loenne[18], V. Loginov[75], C. Loizides[74], X. Lopez[70], E. López Torres[9], A. Lowe[135], P. Luettig[53], M. Lunardon[30], G. Luparello[26], A. Maevskaya[56], M. Mager[36], S. Mahajan[90], S.M. Mahmood[22], A. Maire[55], R.D. Majka[136], M. Malaev[85], I. Maldonado Cervantes[63], L. Malinina[·,iii,66], D. Mal'Kevich[58], P. Malzacher[96], A. Mamonov[98], V. Manko[99], F. Manso[70], V. Manzari[36,103], M. Marchisone[27,65,126], J. Mareš[60], G.V. Margagliotti[26], A. Margotti[104], J. Margutti[57], A. Marín[96], C. Markert[118], M. Marquard[53], N.A. Martin[96], J. Martin Blanco[113], P. Martinengo[36], M.I. Martínez[2], G. Martínez García[113], M. Martinez Pedreira[36], A. Mas[120], S. Masciocchi[96], M. Masera[27], A. Masoni[105], L. Massacrier[113], A. Mastroserio[33], A. Matyja[117], C. Mayer[117], J. Mazer[125], M.A. Mazzoni[108], D. Mcdonald[122], F. Meddi[24], Y. Melikyan[75], A. Menchaca-Rocha[64], E. Meninno[31], J. Mercado Pérez[93], M. Meres[39], Y. Miake[128],

JHEP03(2016)081

M.M. Mieskolainen[46] , K. Mikhaylov[66,58] , L. Milano[36] , J. Milosevic[22] , L.M. Minervini[103,23] , A. Mischke[57] , A.N. Mishra[49] , D. Miśkowiec[96] , J. Mitra[132] , C.M. Mitu[62] , N. Mohammadi[57] , B. Mohanty[79,132] , L. Molnar[55,113] , L. Montaño Zetina[11] , E. Montes[10] , D.A. Moreira De Godoy[54,113] , L.A.P. Moreno[2] , S. Moretto[30] , A. Morreale[113] , A. Morsch[36] , V. Muccifora[72] , E. Mudnic[116] , D. Mühlheim[54] , S. Muhuri[132] , M. Mukherjee[132] , J.D. Mulligan[136] , M.G. Munhoz[120] , R.H. Munzer[92,37] , S. Murray[65] , L. Musa[36] , J. Musinsky[59] , B. Naik[48] , R. Nair[77] , B.K. Nandi[48] , R. Nania[104] , E. Nappi[103] , M.U. Naru[16] , H. Natal da Luz[120] , C. Nattrass[125] , K. Nayak[79] , T.K. Nayak[132] , S. Nazarenko[98] , A. Nedosekin[58] , L. Nellen[63] , F. Ng[122] , M. Nicassio[96] , M. Niculescu[62] , J. Niedziela[36] , B.S. Nielsen[80] , S. Nikolaev[99] , S. Nikulin[99] , V. Nikulin[85] , F. Noferini[12,104] , P. Nomokonov[66] , G. Nooren[57] , J.C.C. Noris[2] , J. Norman[124] , A. Nyanin[99] , J. Nystrand[18] , H. Oeschler[93] , S. Oh[136] , S.K. Oh[67] , A. Ohlson[36] , A. Okatan[69] , T. Okubo[47] , L. Olah[135] , J. Oleniacz[133] , A.C. Oliveira Da Silva[120] , M.H. Oliver[136] , J. Onderwaater[96] , C. Oppedisano[110] , R. Orava[46] , A. Ortiz Velasquez[63] , A. Oskarsson[34] , J. Otwinowski[117] , K. Oyama[93,76] , M. Ozdemir[53] , Y. Pachmayer[93] , P. Pagano[31] , G. Paić[63] , S.K. Pal[132] , J. Pan[134] , A.K. Pandey[48] , P. Papcun[115] , V. Papikyan[1] , G.S. Pappalardo[106] , P. Pareek[49] , W.J. Park[96] , S. Parmar[87] , A. Passfeld[54] , V. Paticchio[103] , R.N. Patra[132] , B. Paul[100] , T. Peitzmann[57] , H. Pereira Da Costa[15] , E. Pereira De Oliveira Filho[120] , D. Peresunko[99,75] , C.E. Pérez Lara[81] , E. Perez Lezama[53] , V. Peskov[53] , Y. Pestov[5] , V. Petráček[40] , V. Petrov[111] , M. Petrovici[78] , C. Petta[29] , S. Piano[109] , M. Pikna[39] , P. Pillot[113] , O. Pinazza[104,36] , L. Pinsky[122] , D.B. Piyarathna[122] , M. Płoskoń[74] , M. Planinic[129] , J. Pluta[133] , S. Pochybova[135] , P.L.M. Podesta-Lerma[119] , M.G. Poghosyan[84,86] , B. Polichtchouk[111] , N. Poljak[129] , W. Poonsawat[114] , A. Pop[78] , S. Porteboeuf-Houssais[70] , J. Porter[74] , J. Pospisil[83] , S.K. Prasad[4] , R. Preghenella[36,104] , F. Prino[110] , C.A. Pruneau[134] , I. Pshenichnov[56] , M. Puccio[27] , G. Puddu[25] , P. Pujahari[134] , V. Punin[98] , J. Putschke[134] , H. Qvigstad[22] , A. Rachevski[109] , S. Raha[4] , S. Rajput[90] , J. Rak[123] , A. Rakotozafindrabe[15] , L. Ramello[32] , F. Rami[55] , R. Raniwala[91] , S. Raniwala[91] , S.S. Räsänen[46] , B.T. Rascanu[53] , D. Rathee[87] , K.F. Read[125,84] , K. Redlich[77] , R.J. Reed[134] , A. Rehman[18] , P. Reichelt[53] , F. Reidt[93,36] , X. Ren[7] , R. Renfordt[53] , A.R. Reolon[72] , A. Reshetin[56] , J.-P. Revol[12] , K. Reygers[93] , V. Riabov[85] , R.A. Ricci[73] , T. Richert[34] , M. Richter[22] , P. Riedler[36] , W. Riegler[36] , F. Riggi[29] , C. Ristea[62] , E. Rocco[57] , M. Rodríguez Cahuantzi[2,11] , A. Rodriguez Manso[81] , K. Røed[22] , E. Rogochaya[66] , D. Rohr[43] , D. Röhrich[18] , R. Romita[124] , F. Ronchetti[72,36] , L. Ronflette[113] , P. Rosnet[70] , A. Rossi[30,36] , F. Roukoutakis[88] , A. Roy[49] , C. Roy[55] , P. Roy[100] , A.J. Rubio Montero[10] , R. Rui[26] , R. Russo[27] , E. Ryabinkin[99] , Y. Ryabov[85] , A. Rybicki[117] , S. Sadovsky[111] , K. Šafařík[36] , B. Sahlmuller[53] , P. Sahoo[49] , R. Sahoo[49] , S. Sahoo[61] , P.K. Sahu[61] , J. Saini[132] , S. Sakai[72] , M.A. Saleh[134] , J. Salzwedel[20] , S. Sambyal[90] , V. Samsonov[85] , L. Šándor[59] , A. Sandoval[64] , M. Sano[128] , D. Sarkar[132] , E. Scapparone[104] , F. Scarlassara[30] , C. Schiaua[78] , R. Schicker[93] , C. Schmidt[96] , H.R. Schmidt[35] , S. Schuchmann[53] , J. Schukraft[36] , M. Schulc[40] , T. Schuster[136] , Y. Schutz[36,113] , K. Schwarz[96] , K. Schweda[96] , G. Scioli[28] , E. Scomparin[110] , R. Scott[125] , M. Šefčík[41] , J.E. Seger[86] , Y. Sekiguchi[127] , D. Sekihata[47] , I. Selyuzhenkov[96] , K. Senosi[65] , S. Senyukov[3,36] , E. Serradilla[10,64] , A. Sevcenco[62] , A. Shabanov[56] , A. Shabetai[113] , O. Shadura[3] , R. Shahoyan[36] , A. Shangaraev[111] , A. Sharma[90] , M. Sharma[90] , M. Sharma[90] , N. Sharma[125] , K. Shigaki[47] , K. Shtejer[9,27] , Y. Sibiriak[99] , S. Siddhanta[105] , K.M. Sielewicz[36] , T. Siemiarczuk[77] , D. Silvermyr[84,34] , C. Silvestre[71] , G. Simatovic[129] , G. Simonetti[36] , R. Singaraju[132] , R. Singh[79] , S. Singha[132,79] , V. Singhal[132] , B.C. Sinha[132] , T. Sinha[100] , B. Sitar[39] , M. Sitta[32] , T.B. Skaali[22] , M. Slupecki[123] , N. Smirnov[136] , R.J.M. Snellings[57] , T.W. Snellman[123] , C. Søgaard[34] , J. Song[95] , M. Song[137] , Z. Song[7] , F. Soramel[30] , S. Sorensen[125] , F. Sozzi[96] , M. Spacek[40] , E. Spiriti[72] , I. Sputowska[117] , M. Spyropoulou-Stassinaki[88] , J. Stachel[93] , I. Stan[62] , G. Stefanek[77] , E. Stenlund[34] , G. Steyn[65] , J.H. Stiller[93] , D. Stocco[113] , P. Strmen[39] , A.A.P. Suaide[120] , T. Sugitate[47] , C. Suire[51] ,

JHEP03(2016)081

M. Suleymanov[16], M. Suljic[26,i], R. Sultanov[58], M. Šumbera[83], A. Szabo[39], A. Szanto de Toledo[120,i], I. Szarka[39], A. Szczepankiewicz[36], M. Szymanski[133], U. Tabassam[16], J. Takahashi[121], G.J. Tambave[18], N. Tanaka[128], M.A. Tangaro[33], M. Tarhini[51], M. Tariq[19], M.G. Tarzila[78], A. Tauro[36], G. Tejeda Muñoz[2], A. Telesca[36], K. Terasaki[127], C. Terrevoli[30], B. Teyssier[130], J. Thäder[74], D. Thomas[118], R. Tieulent[130], A.R. Timmins[122], A. Toia[53], S. Trogolo[27], G. Trombetta[33], V. Trubnikov[3], W.H. Trzaska[123], T. Tsuji[127], A. Tumkin[98], R. Turrisi[107], T.S. Tveter[22], K. Ullaland[18], A. Uras[130], G.L. Usai[25], A. Utrobicic[129], M. Vajzer[83], M. Vala[59], L. Valencia Palomo[70], S. Vallero[27], J. Van Der Maarel[57], J.W. Van Hoorne[36], M. van Leeuwen[57], T. Vanat[83], P. Vande Vyvre[36], D. Varga[135], A. Vargas[2], M. Vargyas[123], R. Varma[48], M. Vasileiou[88], A. Vasiliev[99], A. Vauthier[71], V. Vechernin[131], A.M. Veen[57], M. Veldhoen[57], A. Velure[18], M. Venaruzzo[73], E. Vercellin[27], S. Vergara Limón[2], R. Vernet[8], M. Verweij[134], L. Vickovic[116], G. Viesti[30,i], J. Viinikainen[123], Z. Vilakazi[126], O. Villalobos Baillie[101], A. Villatoro Tello[2], A. Vinogradov[99], L. Vinogradov[131], Y. Vinogradov[98,i], T. Virgili[31], V. Vislavicius[34], Y.P. Viyogi[132], A. Vodopyanov[66], M.A. Völkl[93], K. Voloshin[58], S.A. Voloshin[134], G. Volpe[135], B. von Haller[36], I. Vorobyev[37,92], D. Vranic[96,36], J. Vrláková[41], B. Vulpescu[70], A. Vyushin[98], B. Wagner[18], J. Wagner[96], H. Wang[57], M. Wang[7,113], D. Watanabe[128], Y. Watanabe[127], M. Weber[112,36], S.G. Weber[96], D.F. Weiser[93], J.P. Wessels[54], U. Westerhoff[54], A.M. Whitehead[89], J. Wiechula[35], J. Wikne[22], M. Wilde[54], G. Wilk[77], J. Wilkinson[93], M.C.S. Williams[104], B. Windelband[93], M. Winn[93], C.G. Yaldo[134], H. Yang[57], P. Yang[7], S. Yano[47], C. Yasar[69], Z. Yin[7], H. Yokoyama[128], I.-K. Yoo[95], J.H. Yoon[50], V. Yurchenko[3], I. Yushmanov[99], A. Zaborowska[133], V. Zaccolo[80], A. Zaman[16], C. Zampolli[104], H.J.C. Zanoli[120], S. Zaporozhets[66], N. Zardoshti[101], A. Zarochentsev[131], P. Závada[60], N. Zaviyalov[98], H. Zbroszczyk[133], I.S. Zgura[62], M. Zhalov[85], H. Zhang[18], X. Zhang[74], Y. Zhang[7], C. Zhang[57], Z. Zhang[7], C. Zhao[22], N. Zhigareva[58], D. Zhou[7], Y. Zhou[80], Z. Zhou[18], H. Zhu[18], J. Zhu[113,7], A. Zichichi[28,12], A. Zimmermann[93], M.B. Zimmermann[54,36], G. Zinovjev[3], M. Zyzak[43]

[i] *Deceased*

[ii] *Also at: Georgia State University, Atlanta, Georgia, United States*

[iii] *Also at: M.V. Lomonosov Moscow State University, D.V. Skobeltsyn Institute of Nuclear, Physics, Moscow, Russia*

[1] *A.I. Alikhanyan National Science Laboratory (Yerevan Physics Institute) Foundation, Yerevan, Armenia*

[2] *Benemérita Universidad Autónoma de Puebla, Puebla, Mexico*

[3] *Bogolyubov Institute for Theoretical Physics, Kiev, Ukraine*

[4] *Bose Institute, Department of Physics and Centre for Astroparticle Physics and Space Science (CAPSS), Kolkata, India*

[5] *Budker Institute for Nuclear Physics, Novosibirsk, Russia*

[6] *California Polytechnic State University, San Luis Obispo, California, United States*

[7] *Central China Normal University, Wuhan, China*

[8] *Centre de Calcul de l'IN2P3, Villeurbanne, France*

[9] *Centro de Aplicaciones Tecnológicas y Desarrollo Nuclear (CEADEN), Havana, Cuba*

[10] *Centro de Investigaciones Energéticas Medioambientales y Tecnológicas (CIEMAT), Madrid, Spain*

[11] *Centro de Investigación y de Estudios Avanzados (CINVESTAV), Mexico City and Mérida, Mexico*

[12] *Centro Fermi - Museo Storico della Fisica e Centro Studi e Ricerche "Enrico Fermi", Rome, Italy*

[13] *Chicago State University, Chicago, Illinois, U.S.A.*

[14] *China Institute of Atomic Energy, Beijing, China*

[15] *Commissariat à l'Energie Atomique, IRFU, Saclay, France*

JHEP03(2016)081

[16] COMSATS Institute of Information Technology (CIIT), Islamabad, Pakistan
[17] Departamento de Física de Partículas and IGFAE, Universidad de Santiago de Compostela, Santiago de Compostela, Spain
[18] Department of Physics and Technology, University of Bergen, Bergen, Norway
[19] Department of Physics, Aligarh Muslim University, Aligarh, India
[20] Department of Physics, Ohio State University, Columbus, Ohio, United States
[21] Department of Physics, Sejong University, Seoul, South Korea
[22] Department of Physics, University of Oslo, Oslo, Norway
[23] Dipartimento di Elettrotecnica ed Elettronica del Politecnico, Bari, Italy
[24] Dipartimento di Fisica dell'Università 'La Sapienza' and Sezione INFN Rome, Italy
[25] Dipartimento di Fisica dell'Università and Sezione INFN, Cagliari, Italy
[26] Dipartimento di Fisica dell'Università and Sezione INFN, Trieste, Italy
[27] Dipartimento di Fisica dell'Università and Sezione INFN, Turin, Italy
[28] Dipartimento di Fisica e Astronomia dell'Università and Sezione INFN, Bologna, Italy
[29] Dipartimento di Fisica e Astronomia dell'Università and Sezione INFN, Catania, Italy
[30] Dipartimento di Fisica e Astronomia dell'Università and Sezione INFN, Padova, Italy
[31] Dipartimento di Fisica 'E.R. Caianiello' dell'Università and Gruppo Collegato INFN, Salerno, Italy
[32] Dipartimento di Scienze e Innovazione Tecnologica dell'Università del Piemonte Orientale and Gruppo Collegato INFN, Alessandria, Italy
[33] Dipartimento Interateneo di Fisica 'M. Merlin' and Sezione INFN, Bari, Italy
[34] Division of Experimental High Energy Physics, University of Lund, Lund, Sweden
[35] Eberhard Karls Universität Tübingen, Tübingen, Germany
[36] European Organization for Nuclear Research (CERN), Geneva, Switzerland
[37] Excellence Cluster Universe, Technische Universität München, Munich, Germany
[38] Faculty of Engineering, Bergen University College, Bergen, Norway
[39] Faculty of Mathematics, Physics and Informatics, Comenius University, Bratislava, Slovakia
[40] Faculty of Nuclear Sciences and Physical Engineering, Czech Technical University in Prague, Prague, Czech Republic
[41] Faculty of Science, P.J. Šafárik University, Košice, Slovakia
[42] Faculty of Technology, Buskerud and Vestfold University College, Vestfold, Norway
[43] Frankfurt Institute for Advanced Studies, Johann Wolfgang Goethe-Universität Frankfurt, Frankfurt, Germany
[44] Gangneung-Wonju National University, Gangneung, South Korea
[45] Gauhati University, Department of Physics, Guwahati, India
[46] Helsinki Institute of Physics (HIP), Helsinki, Finland
[47] Hiroshima University, Hiroshima, Japan
[48] Indian Institute of Technology Bombay (IIT), Mumbai, India
[49] Indian Institute of Technology Indore, Indore (IITI), India
[50] Inha University, Incheon, South Korea
[51] Institut de Physique Nucléaire d'Orsay (IPNO), Université Paris-Sud, CNRS-IN2P3, Orsay, France
[52] Institut für Informatik, Johann Wolfgang Goethe-Universität Frankfurt, Frankfurt, Germany
[53] Institut für Kernphysik, Johann Wolfgang Goethe-Universität Frankfurt, Frankfurt, Germany
[54] Institut für Kernphysik, Westfälische Wilhelms-Universität Münster, Münster, Germany
[55] Institut Pluridisciplinaire Hubert Curien (IPHC), Université de Strasbourg, CNRS-IN2P3, Strasbourg, France
[56] Institute for Nuclear Research, Academy of Sciences, Moscow, Russia
[57] Institute for Subatomic Physics of Utrecht University, Utrecht, Netherlands
[58] Institute for Theoretical and Experimental Physics, Moscow, Russia
[59] Institute of Experimental Physics, Slovak Academy of Sciences, Košice, Slovakia
[60] Institute of Physics, Academy of Sciences of the Czech Republic, Prague, Czech Republic
[61] Institute of Physics, Bhubaneswar, India
[62] Institute of Space Science (ISS), Bucharest, Romania
[63] Instituto de Ciencias Nucleares, Universidad Nacional Autónoma de México, Mexico City, Mexico

JHEP03(2016)081

[64] Instituto de Física, Universidad Nacional Autónoma de México, Mexico City, Mexico
[65] iThemba LABS, National Research Foundation, Somerset West, South Africa
[66] Joint Institute for Nuclear Research (JINR), Dubna, Russia
[67] Konkuk University, Seoul, South Korea
[68] Korea Institute of Science and Technology Information, Daejeon, South Korea
[69] KTO Karatay University, Konya, Turkey
[70] Laboratoire de Physique Corpusculaire (LPC), Clermont Université, Université Blaise Pascal, CNRS-IN2P3, Clermont-Ferrand, France
[71] Laboratoire de Physique Subatomique et de Cosmologie, Université Grenoble-Alpes, CNRS-IN2P3, Grenoble, France
[72] Laboratori Nazionali di Frascati, INFN, Frascati, Italy
[73] Laboratori Nazionali di Legnaro, INFN, Legnaro, Italy
[74] Lawrence Berkeley National Laboratory, Berkeley, California, United States
[75] Moscow Engineering Physics Institute, Moscow, Russia
[76] Nagasaki Institute of Applied Science, Nagasaki, Japan
[77] National Centre for Nuclear Studies, Warsaw, Poland
[78] National Institute for Physics and Nuclear Engineering, Bucharest, Romania
[79] National Institute of Science Education and Research, Bhubaneswar, India
[80] Niels Bohr Institute, University of Copenhagen, Copenhagen, Denmark
[81] Nikhef, Nationaal instituut voor subatomaire fysica, Amsterdam, Netherlands
[82] Nuclear Physics Group, STFC Daresbury Laboratory, Daresbury, United Kingdom
[83] Nuclear Physics Institute, Academy of Sciences of the Czech Republic, Řež u Prahy, Czech Republic
[84] Oak Ridge National Laboratory, Oak Ridge, Tennessee, United States
[85] Petersburg Nuclear Physics Institute, Gatchina, Russia
[86] Physics Department, Creighton University, Omaha, Nebraska, United States
[87] Physics Department, Panjab University, Chandigarh, India
[88] Physics Department, University of Athens, Athens, Greece
[89] Physics Department, University of Cape Town, Cape Town, South Africa
[90] Physics Department, University of Jammu, Jammu, India
[91] Physics Department, University of Rajasthan, Jaipur, India
[92] Physik Department, Technische Universität München, Munich, Germany
[93] Physikalisches Institut, Ruprecht-Karls-Universität Heidelberg, Heidelberg, Germany
[94] Purdue University, West Lafayette, Indiana, United States
[95] Pusan National University, Pusan, South Korea
[96] Research Division and ExtreMe Matter Institute EMMI, GSI Helmholtzzentrum für Schwerionenforschung, Darmstadt, Germany
[97] Rudjer Bošković Institute, Zagreb, Croatia
[98] Russian Federal Nuclear Center (VNIIEF), Sarov, Russia
[99] Russian Research Centre Kurchatov Institute, Moscow, Russia
[100] Saha Institute of Nuclear Physics, Kolkata, India
[101] School of Physics and Astronomy, University of Birmingham, Birmingham, United Kingdom
[102] Sección Física, Departamento de Ciencias, Pontificia Universidad Católica del Perú, Lima, Peru
[103] Sezione INFN, Bari, Italy
[104] Sezione INFN, Bologna, Italy
[105] Sezione INFN, Cagliari, Italy
[106] Sezione INFN, Catania, Italy
[107] Sezione INFN, Padova, Italy
[108] Sezione INFN, Rome, Italy
[109] Sezione INFN, Trieste, Italy
[110] Sezione INFN, Turin, Italy
[111] SSC IHEP of NRC Kurchatov institute, Protvino, Russia
[112] Stefan Meyer Institut für Subatomare Physik (SMI), Vienna, Austria
[113] SUBATECH, Ecole des Mines de Nantes, Université de Nantes, CNRS-IN2P3, Nantes, France

JHEP03(2016)081

[114] *Suranaree University of Technology, Nakhon Ratchasima, Thailand*
[115] *Technical University of Košice, Košice, Slovakia*
[116] *Technical University of Split FESB, Split, Croatia*
[117] *The Henryk Niewodniczanski Institute of Nuclear Physics, Polish Academy of Sciences, Cracow, Poland*
[118] *The University of Texas at Austin, Physics Department, Austin, Texas, U.S.A.*
[119] *Universidad Autónoma de Sinaloa, Culiacán, Mexico*
[120] *Universidade de São Paulo (USP), São Paulo, Brazil*
[121] *Universidade Estadual de Campinas (UNICAMP), Campinas, Brazil*
[122] *University of Houston, Houston, Texas, United States*
[123] *University of Jyväskylä, Jyväskylä, Finland*
[124] *University of Liverpool, Liverpool, United Kingdom*
[125] *University of Tennessee, Knoxville, Tennessee, United States*
[126] *University of the Witwatersrand, Johannesburg, South Africa*
[127] *University of Tokyo, Tokyo, Japan*
[128] *University of Tsukuba, Tsukuba, Japan*
[129] *University of Zagreb, Zagreb, Croatia*
[130] *Université de Lyon, Université Lyon 1, CNRS/IN2P3, IPN-Lyon, Villeurbanne, France*
[131] *V. Fock Institute for Physics, St. Petersburg State University, St. Petersburg, Russia*
[132] *Variable Energy Cyclotron Centre, Kolkata, India*
[133] *Warsaw University of Technology, Warsaw, Poland*
[134] *Wayne State University, Detroit, Michigan, United States*
[135] *Wigner Research Centre for Physics, Hungarian Academy of Sciences, Budapest, Hungary*
[136] *Yale University, New Haven, Connecticut, United States*
[137] *Yonsei University, Seoul, South Korea*
[138] *Zentrum für Technologietransfer und Telekommunikation (ZTT), Fachhochschule Worms, Worms, Germany*

JHEP03(2016)081